2704

CONTRACTOR REPORT

SAND84–7213
Unlimited Release
UC–70

Nevada Nuclear Waste Storage Investigations Project

Interaction of Nuclear Waste Panels With Shafts and Access Ramps for a Potential Repository at Yucca Mountain

C. M. St. John
Agbabian Associates
250 North Nash St.
El Segundo, CA 90245

Prepared by Sandia National Laboratories Albuquerque, New Mexico 87185
and Livermore, California 94550 for the United States Department of Energy
under Contract DE-AC04-76DP00789

Printed September 1987

"Prepared by Nevada Nuclear Waste Storage Investigations (NNWSI) Project participants as part of the Civilian Radioactive Waste Management Program (CRWM). The NNWSI Project is managed by the Waste Management Project Office (WMPO) of the U. S. Department of Energy, Nevada Operations Office (DOE/NV). NNWSI Project work is sponsored by the Office of Geologic Repositories (OGR) of the DOE Office of Civilian Radioactive Waste Management (OCRWM)."

Issued by Sandia National Laboratories, operated for the United States Department of Energy by Sandia Corporation.

Printed in the United States of America
Available from
National Technical Information Service
U.S. Department of Commerce
5285 Port Royal Road
Springfield, VA 22161

NTIS price codes
Printed copy: A04
Microfiche copy: A01

SAND84-7213

Unlimited Release
Printed September 1987

Interaction of Nuclear Waste Panels With Shafts And Access Ramps for a Potential Repository at Yucca Mountain

by

Christopher M. St. John*
Agbabian Associates

for

Sandia National Laboratories
P. O. Box 5800
Albuquerque, New Mexico

Under Sandia Contract: 52-3876

Sandia Contract Monitor
A. Mansure
Geotechnical Design Division 6314

ABSTRACT

A series of two-dimensional and three-dimensional analyses of a potential nuclear waste repository at Yucca Mountain were performed with the objective of estimating the thermal stresses that would be experienced at the possible locations of shafts or ramps providing access to the repository horizon. Two alternative assumptions were made for the initial state of stress, and calculations were performed to investigate behavior at repository scale. The computed states of stress were also used as boundary conditions for a series of analyses of the access ramps and vertical shafts.

The results of the repository scale analyses indicated that there is a region above the repository horizon where the horizontal stresses are reduced as a consequence of the thermal loads imposed by waste emplacement. If the initial state of stress is relatively low then the total horizontal stresses near the ground surface above the repository may be tensile. An evaluation of the total stress state relative to the strength of the rock matrix and vertical and near vertical joints indicates that there is no potential for development of new fractures in the matrix, but joints near the surface could be activated if the initial stress state is low. It is observed however that there is no indication that the predicted regions of joint activation would be detrimental to repository performance.

Analysis of the access ramps also indicated that, under the assumed set of conditions, there would be no development of new fractures in the rock matrix but there is some potential for activation of joints in the roof and sidewalls of the openings. Generally, the regions of activation were very localized and do not appear to represent any threat to opening stability. The state of stress in shaft liners was evaluated using a simple model accounting for interaction between the rock mass and the liner after thermal loading of the repository. It was concluded that there is a potential for development of horizontal cracks in the liner due to extension of the shaft. Although such cracking may not be detrimental to the shaft performance, the effects of thermal loading should be considered during shaft design.

*Currently with J. F. T. Agapito & Associates, Inc.
27520 Hawthorne Blvd., Suite 295,
Rolling Hills Estates, CA 90274

ACKNOWLEDGMENTS

This study was initiated by Arthur Mansure, under Sandia Contract 52-3876 with Agbabian Associates, where analyses were performed by T. F. Zahrah and K. Kim under the direction of the author of this report. Modifications in response to technical and editorial review by the staff of Sandia National Laboratories were completed under Sandia Contract 25-8908 with J. F. T. Agapito & Associates, Inc. Kathy Wright was responsible for report preparation.

TABLE OF CONTENTS

LIST OF FIGURES

LIST OF FIGURES (CONTINUED)

LIST OF TABLES

1.0 INTRODUCTION

1.1 Purpose and Justification

The work described in this report was performed for Sandia National Laboratories (SNL) as a part of the Nevada Nuclear Waste Storage Investigations (NNWSI) project. SNL is one of the principal organizations participating in the project, which is managed by the U.S. Department of Energy's (DOE's) Nevada Operations Office. The project is a part of the DOE's program to safely dispose of the radioactive waste from nuclear power plants.

The DOE has determined that the safest and most feasible method currently known for the disposal of such wastes is to emplace them in mined geologic repositories. To that end, the NNWSI project is conducting detailed studies of Yucca Mountain, which is an area on and near the Nevada Test Site (NTS) in southern Nevada, with a view determining the feasibility of developing a repository in tuff.

The emplacement of high-level waste induces stresses that affect the stability of the accesses to the underground facility. The objective of the work described in this report was to complete a preliminary investigation of the potential impact of thermally induced stresses on the stability of shaft or ramp accesses to a nuclear waste repository in tuff. Two alternative shaft sitings were considered: a central location within a shaft pillar and a location on the periphery of the repository. For the purpose of these initial analyses, the ramps were assumed to provide access to a central shaft pillar. In the current design for a repository at Yucca Mountain (MacDougall, 1986), ramps descend to the periphery of the repository and do not pass above areas of waste emplacement. The stress changes experienced by those ramps is expected to be significantly less than the case discussed here. Similarly, the stress changes induced in the shaft liners are anticipated to be more moderate than discussed here because currently proposed shaft locations are further from the waste emplacement panels.

The preliminary investigation described in this report is restricted to consideration of a single waste form and one emplacement configuration. The waste chosen was pressurized water reactor spent fuel (PWR SF). A horizontal configuration mode was considered specifically, but the differences from other emplacement modes are inconsequential at the scale of the analysis performed here. On this scale, the areal power density (APD) and waste characteristics are much more important than the emplacement mode.

This report consists of five parts. Following this introduction, the problem is described in detail: specifically, the site layout, rock mass properties, and the waste forms are defined. The methods used for analysis are described and some preliminary analytical results are presented in Section 3. Section 4 presents results of analyses of a repository comprised of four waste

panels, and analyses of ramps and vertical shafts that provide access to the repository horizon are described. The final part consists of general conclusions.

2. PROBLEM DEFINITION

Data for the present investigation are drawn from four sources. Geometrical data are from a Keystone Memorandum (Shirley, 1983a), that defines reference waste emplacement geometries for various waste types and emplacement modes, as of June 1983. Waste characteristic data are from a second Keystone Memorandum (Shirley, 1983b), that defines the thermal power decay and energy release functions for candidate waste forms. Site characteristics, including stratigraphic data, physical properties of the host rock, and the preconstruction stress state, are from a Keystone memorandum by Nimick et al., (1984). These and other data are summarized in this section.

2.1 Geometrical Definition

The repository models involve four different underground components or structures: the waste panels, the shaft pillar, access ramps, and shafts. As will be explained in Section 4, details of location and number of panels are anticipated to have relatively little impact on the stress states in rock media for these analyses, so long as the individual panels are wide in comparison to the emplacement horizon depth. Accordingly, a rather simple layout can be used as a basis for the preliminary investigations discussed in this study. Such a layout is depicted schematically in Figure 1. That layout incorporates four emplacement panels at a depth of 295.7 m, with a single central pillar dividing the repository horizon into two parts. Consistent with data given by Shirley (1983a), each panel for horizontal emplacement of waste containers is assumed to comprise 13 long horizontal holes on each side of a central emplacement drift. The center-to-center hole spacing is 36 m, and the nominal panel width is assumed to be 504 m. The first horizontal hole is thus 36 m from the panel boundary, giving a hole spacing of 72 m between boreholes in adjacent panels. Within the pillar between the panels there are two access drifts, 16 m apart, that run parallel to the emplacement holes.

In this study, it was assumed that a pillar 200 m wide would be located at the center of the repository. Three accesses to the repository horizon were analyzed. First, it was assumed that a shaft may be located at the center of the pillar. The second assumed shaft location was 100 m beyond the panel boundary. Finally, it was assumed that access might be effected via a ramp connecting the shaft pillar and ground surface. It was further assumed that such a ramp would be inclined at 10° to the plane of the horizontal emplacement panels and intersect the shaft pillar at the side remote from the ramp entrance. The arrangement of the shaft pillar, panels, and ramp is illustrated in Figure 1.

2.2 Material Definitions

The following thermomechanical properties and parameters for the rock mass were used in the analyses.

Thermal conductivity	K	= 1.85 W/m°C
Heat capacity	ρC	= 2.17 MJ/m³°C
Density (average)	ρ	= 2093 kg/m³
Elastic modulus	E	= 15.1 GPa
Poisson's ratio	ν	= 0.2
Coefficient of thermal expansion	α	= 10.7 x 10^{-6}/°C
Intact matrix cohesion	C_m	= 22.1 MPa
Intact matrix friction angle	ϕ_m	= 29.2°
Uniaxial compressive strength	q_m	= 75.3 MPa
Uniaxial tensile strength	σ_t	= -6.5 MPa
Joint cohesion	C_j	= 1.0 MPa
Joint friction angle	σ_j	= 39°
Joint orientation		90° (vertical)

In Appendix A these data are compared with current baseline data assembled by Zeuch and Eatough (1986).

2.3 Waste Form and Heat Source Definition

Keystone 6310-83-2 gives the following normalized thermal power decay function for ten year old PWR SF:

$$y(t) = 0.7707 \exp(-0.02689\ t) + 0.1932 \exp(-0.002199\ t) + 0.02163 \exp(-0.00005343\ t)$$

in which the normalized power y is expressed as a function of t, the time in years since emplacement in the repository.

The initial thermal power of each heat source can be calculated from the APD, the panel geometry, and the heat capacity of the rock. In this investigation, the APD was assumed to average 57 kW/acre (14.1 W/m²) over each panel. For the geometry shown in Figure 1, initial thermal load per meter along each hole is

$$P_o = \frac{504 \cdot APD}{13} \text{ (W/m)}$$

in which the APD is defined in W/m². Hence, the initial strength of a heat source simulating the presence of the waste containers in the emplacement boreholes is:

$$Q_o = \frac{P_o}{\rho C} = 7936 \text{ °C m}^3\text{/yr per meter}$$

3. METHOD OF ANALYSIS

The stress state in a rock mass after the introduction of heat sources is the combined result of initial overburden pressure and induced thermal loading. In this preliminary study, it was assumed that material behavior is linear elastic and that overburden and thermal stresses are uncoupled. Consequently, superposition of initial stresses and thermal stresses can be used.

The first step in this study was to calculate the stress distribution around the underground facility, considering two initial stress states. Thermal stress calculations were performed with the objective of predicting the thermally induced stress and the computed stresses were then superimposed on one of the two initial stress states. These thermomechanical analyses were performed using a two-dimensional boundary-element code and a three-dimensional semianalytical procedure, both of which are described in Section 3.2.

After the combined thermomechanical and initial stresses were computed, they were used to define boundary conditions for further analyses of stresses and displacements around the access ramp and shafts. Two-dimensional boundary-element analyses were performed for the access ramp, and a closed-form solution for a lined circular shaft was used for the shaft studies.

Details of calculation procedures for the initial stresses and brief descriptions of various stress analysis codes are presented in Section 3.1 and 3.2, respectively. Then, in Section 3.3, a comparison is drawn between the results of two- and three-dimensional analyses, and the need for three-dimensional analyses is discussed. Finally, in Section 3.4, the procedures for evaluation of the computed stress states are described.

3.1 Initial Stresses

Since linear behavior of materials is assumed, stresses due to temperature changes and those due to initial overburden pressure can be superposed. For the initial stresses, the vertical stress σ_v at a point is given by

$$\sigma_v = - \rho g h \ , \tag{1}$$

in which h is the elevation of the point relative to the surface ($h < 0$) and ρ is the average density of the rock mass.

Assuming that lateral displacements are prevented, linear elasticity theory predicts that the horizontal stress σ_h is

$$\sigma_h = \left(\frac{\nu}{1 - \nu}\right) \sigma_v \ , \tag{2}$$

in which ν is the Poisson's ratio. According to that model, σ_h is equal in all directions. In practice, the stress state within rock masses does not conform exactly to the simple linear elasticity model. Nonlinear deformation and the tectonic environment together result in stress states that typically exceed that predicted by the elastic model. The second initial stress state used in this study is based on review of several studies of the relationship between horizontal and vertical stresses. The unit evaluation studies (Johnstone et al., 1984) used the following empirical function:

$$\sigma_h = \text{MIN}\left[(0.55 - \frac{150}{h})\ \sigma_v,\ 2.4\ \sigma_v\right] , \qquad (3)$$

in which the depth, h, is defined in meters

In the remainder of this report, the analyses in which Equations 1 and 2 are used to define initial stresses are designated Case 1. Analyses in which Equations 1 and 3 are used are designated Case 2. Variations of horizontal stresses and vertical stresses with respect to depth are plotted for both cases in Figure 2. From that figure, it is evident that the initial horizontal stresses at repository depth will be rather close to the vertical stresses in Case 2, but for Case 1 the horizontal stresses will be much less than the vertical stresses.

3.2 Computer Codes for Stress Analysis

The objectives of the stress analyses performed were to investigate the general response of the rock mass to the thermal loading resulting from waste emplacement and to evaluate the potential impact on shafts and access ramps. Details of excavations on the repository horizon are not simulated when evaluating the large-scale response; therefore, the repository can be represented very simply as a number of heat sources embedded within a continuous half-space. The results of such large-scale analyses can be used subsequently in detailed models of the shafts and ramps.

In the two computer codes applied for large-scale thermomechanical analysis, use is made of analytical solutions for determining the temperature, displacements, and stresses in the vicinity of a heat source. These solutions are based on the assumption that the medium is homogeneous and linearly elastic and that heat is generated either along a line or at a point. The two codes are HEFF and STRES3D.

- HEFF is a two-dimensional boundary-element code that uses the analytical solution for temperatures, displacements, and stresses around constant or exponentially decaying infinite line heat sources. Boundary elements can be used to represent any boundary, including the ground surface above the repository horizon or the walls, floor and

roof of an underground excavation. HEFF has been documented by Brady (1980).

- o STRES3D is a three-dimensional, semianalytical code that uses the analytical solution for temperatures, displacements, and stresses around constant or exponentially decaying point heat sources. The effect of the ground surface is accounted for by the method of images and superposition of distributed shear forces across the free surface. STRES3D has been documented by St. John and Christianson (1980).

Two computer codes were used for the smaller-scale calculations (i.e., stability of the shaft and ramp). The stability of the ramp was studied using HEFF. Strictly, those analyses should be performed using a three-dimensional model accounting for the complete state of stress to which the ramp is subjected. However, for these preliminary analyses it was considered appropriate to calculate the stresses in the plane of a cross-section normal to the axis of the ramp and to assume plane strain conditions. HEFF was not used for analysis of the possible effect of thermal loading on the stability of a lined shaft because only homogeneous media can be modeled using that code. Instead, a special- purpose code, SHAFT, was used.

- o SHAFT is a code for analyzing the state of stress in a liner within a long circular opening, such as a tunnel or shaft, when the state of the stress in the surrounding rock mass is changed by thermal loads or other causes. The code is based on a closed-form analytical solution for lined holes in a biaxial stress field (St. John and Van Dillen, (1983)).

Input to the SHAFT Code comprises geometrical and material properties of the rock mass and liner, the changes in the principal stresses in the plane of the cross-section of the lined opening and the axial strain. The axial strain under isothermal conditions is derived directly from the stress changes in the surrounding rock mass using the relationship:

$$\epsilon_y = (\Delta\sigma_y - \nu\ (\Delta\sigma_z + \Delta\sigma_x))/E \qquad (4)$$

in which $\Delta\sigma_y$ is the change in the axial, or vertical stress, and $\Delta\sigma_z$ and $\Delta\sigma_x$ the changes in the horizontal stresses and ν and E are the elastic parameters for the rock mass. As discussed below, for the two-dimensional models $\Delta\sigma_z$ is the change in the out-of-plane stress. The assumptions are made that the shaft liner experiences the same axial strain as the rock mass and that the effect of the temperature changes that occur at the shaft locations can be ignored because the changes are small and because the coefficients of linear thermal expansion of the rock mass and the material of the liner are similar.

3.3 Three-Dimensional Effects: Preliminary Analysis

The underground facility is, in fact, three-dimensional, since the waste panels have a finite length in z-direction (the out-of-plane dimension in Figure 1). However, because dimensions of the shafts or ramps in the z-direction are negligible compared to panel dimensions, it is logical to reduce the problem to two dimensions by assuming that the panels extend infinitely in the z-direction.

The validity of the above simplification was checked by comparing the stress distribution for a single, square panel with those for the equivalent two-dimensional cross section. The geometric and thermomechanical parameters and properties for that single panel were the same as defined in Section 2. The panel was assumed to be 504 m square and to be located 295.7 m below the surface. To be consistent with other cases of this preliminary study, it was assumed that the panel contained parallel, horizontal canister holes spaced 36 m apart.

For three-dimensional analysis, the heat generation along each canister hole was concentrated at 13 points along the axis of each hole. Hence, heat generation within the panel was represented by a total of 169 point heat sources. For two-dimensional analysis, each canister hole was represented by a single line source extending infinitely in and out of the plane of the section. Hence in the two-dimensional model heat generation within the panel was represented by 13 line heat sources.

Thermally induced principal stresses on the x-y plane along the centerline of the panel 50 years after emplacement of PWR SF at 57 kW/acre, computed using the STRES3D and HEFF codes, are plotted in Figure 3. The differences between the states of stress computed using the two- and three-dimensional models are relatively minor and would probably decrease if there were additional panels either side of the single panel modeled in the three-dimensional case. Moreover, the stress deviator $(\sigma_1 - \sigma_3)/2$, which is directly related to the failure potential of the rock mass, agrees closely.

For analysis of the shafts and access ramps the out-of-plane stress is important. For two-dimensional models, the out-of-plane stresses can be calculated assuming conditions of complete lateral confinement, i.e.,

$$\Delta\sigma_z = \nu\ (\Delta\sigma_x + \Delta\sigma_y) + \alpha E \cdot \Delta T, \qquad (5)$$

where, as noted earlier, $\Delta\sigma_z$ is the change in the out-of-plane stress, $\Delta\sigma_x$ and $\Delta\sigma_y$ are the changes in the in-plane principal stresses, and ΔT is the temperature change at the point. A comparison of values of the out-of-plane stress computed from the data presented in Figure 3, using Equation 5, is provided in Figure 4. Again, good agreement between the two- and three-dimensional models is observed.

From the above preliminary analyses, it was concluded that three-dimensional effects are likely to be less important than variations due to uncertainties in the site definition, repository layout, or waste characteristics. No further consideration is given to three-dimensional effects even though such calculations can be performed quite easily using the STRES3D code.

3.4 Data Presentation

The method for presenting the results of stress analysis is through evaluation of measures of the local stress state relative to some failure criterion. In another report (St. John, 1987a), calculation of a local factor of safety is described in detail. For the matrix material, described by a Mohr-Coulomb failure criterion, the potential for developing new fractures in the matrix can be assessed by calculating the factor of safety,

$$FS_m = \frac{(\sigma_1' + \sigma_2')\ \sin\phi_m + 2C_m\ \cos\phi_m}{(\sigma'_1 - \sigma'_2)}, \qquad (6)$$

in which σ_1' and σ_2' are, respectively, the more compressive and less compressive in-plane principal stresses (the dash superscript has been adopted to signify that the out-of-plane stress has been ignored when determining the principal stresses for the section). In fact, evaluation of the state of stress computed for the repository model and for the ramps indicated that there is little potential for fracturing the matrix and no results of calculating the factor of safety using equation 6 are presented within this report. Instead, the stresses are compared directly with the uniaxial tensile and compressive strengths of the rock matrix. The same approach is also adopted when discussing the potential for development of fractures in a shaft liner.

For a material with ubiquitous jointing inclined at an angle β with respect to σ_1' and a shear strength defined by a Coulomb friction model, the potential for activation of those joints can be assessed by calculating the factor of safety,

$$FS_j = \frac{((\sigma'_1 + \sigma'_2) - (\sigma'_1 - \sigma'_2)\ \cos\ 2\beta)\ \tan\phi_j + 2C_j}{|(\sigma'_1 - \sigma'_2)\ \sin\ 2\beta|}. \qquad (7)$$

In all cases the joints are assumed to strike normal to the plane of the cross-section. In another report (St. John and Mitchell, 1987) it is demonstrated that this assumption is conservative when evaluating the potential for activation of joints around an underground opening.

4. RESULTS OF ANALYSES

Using the methods described in the previous sections, analyses were performed for the rock mass in the vicinity of the repository, the access ramps, and the shafts. The results of these analyses are summarized in this section. In order to reduce the number of calculations and quantity of data to be presented, representative times with respect to waste emplacement were selected; specifically, 10, 50, and 100 years. These times were chosen to correspond to periods early in the operational life of the facility, late in the waste emplacement phase, and toward the end of the life of the repository. For each time period, the alternative initial stress states defined in Section 3 are considered.

In each case considered, the waste was assumed to be emplaced instantaneously. This assumption is believed to be conservative because the peak temperatures and stresses in the different panels do not occur all at the same time. The actual emplacement schedule will have some short-term effects, but these will quickly disappear and the net effect will be a slight reduction in peak stress values and delay in the responses discussed here. (This is in contrast with the temperature level in the immediate vicinity of a waste canister, which is likely to peak within the first 20 years after emplacement, and is only influenced by other canisters within a few tens of meters.)

4.1 Stress State at the Repository Scale

Thermomechanical analyses were performed using the HEFF code to determine the thermally induced stress in the rock mass, ignoring any effect of excavations either at or above the repository horizon. The geometry for those analyses conformed to that illustrated in Figure 1, with boundary elements at the surface extending 2700 m from the line of symmetry at the center of the repository. The computed values of the induced stresses are illustrated in Figures 5a through 7a. In those figures, as in all other principal stress plots, the magnitude and direction of the in-plane principal stresses are indicated by the crossed vectors. The magnitude of the stresses is indicated by the total length of each vector and the orientation by the direction of the vector. The stresses are compressive unless indicated otherwise by a T (for tension) at the end of the corresponding vector.

Reviewing the results presented in Figure 5a through 7a, it is clear that the effect of thermal loading is to induce high horizontal compressive stresses all around the waste panels and relatively high induced vertical tensile stresses at the edge of the panels. The latter effect is particularly noticeable in the central shaft pillar, since the tensions induced by the panels either side of the center of the repository are superimposed. However, induced vertical tensile stresses are also evident at the outer boundary of the repository and in the vicinity of the access drifts between panels.

In practice, it is the total stress, not the induced stress that will determine the potential for development of new fractures or activation of existing joints. To determine the total stress, the induced stress must be added to the initial stress. Figures 5b through 7b and 5c through 7c illustrate the total stress state for the two assumed initial stress conditions. Addition of the initial stress field eliminates the tensile stress at the edge of the panels, because the induced tensile stresses are less than the initial, compressive, vertical stresses. The compressive stresses in the vicinity of the waste panels are increased, obviously more so in Case 2 in which the initial horizontal stresses are higher.

Several possible modes of behavior of the rock mass should be considered when evaluating the impact of waste emplacement. One is development of new fractures as a result of imposed tensile stresses. It has been noted already that the tensile stresses in the vicinity of the panel are eliminated by the addition of the initial stress field. However, tensile stresses close to the ground surface remain. These stresses, which are primarily horizontal, arise from two causes. The first cause is compensation for the compressive stresses close to the heat sources. The effect would be observed even if the repository were located within an infinite rock mass. The second cause is surface uplift, which will be noticeable only if the repository is located relatively close to the ground surface. It should be observed that the presence of large areas of stress reduction above the repository results, in part, from the assumption that the rock mass behaves as a linearly elastic material. This assumption is conservative, because it causes the models to overestimate the thermal expansion and the thermally induced stresses. Despite the conservatism, the stresses throughout the rock mass are relatively low and there is no indication that new fractures in the rock mass would be created under either tensile or compressive stress fields.

To evaluate the potential importance of the tensile stresses, the maximum value calculated at any joint along the ground surface above the repository is plotted as a function of time in Figure 8. Note that after 100 years the maximum tensile stress is still less than half the intact strength of the rock. Hence, there is little potential for development of new fractures due to tensile loads. Also, tensile stresses are not likely to develop because the rock mass contains preexisting fractures that possess limited, if any, tensile strength.

Other possible behavior modes are development of new fractures due to compressive stresses--through crushing or shear failure--and slip along preexisting fracture surfaces. These two behavior modes were analyzed, in the manner explained in Section 3.4, by calculating the factors of safety for both the matrix and preexisting joints. These calculations indicated that for the assumed set of material properties the potential for joint activation is generally greater than the potential for matrix failure. Hence, only results of

evaluation of the potential for joint activation are presented in the discussion that follows.

In Figures 9 and 10 contours of the factor of safety for vertical joints with properties defined in section 2.2 are presented for the three sample times (10, 50, and 100 years). In the first of these figures, which refers to the low initial stress state (Case 1), potential activation of vertical joints is seen above the panels 50 and 100 years after waste emplacement. This behavior reflects the reduction in the horizontal stresses due to the induced tensile thermal stresses. When the higher initial horizontal stresses (Case 2) are assumed, joint activation is largely inhibited (Figure 10).

For the two initial stress states the joint activation potential 100 years after emplacement was also examined for joints having inclination of 14° either way from the vertical direction. Results of those evaluations are illustrated in Figure 11. In that figure it may be observed that towards the center of the repository the potential for activation is slightly higher for joints inclined at an angle of 14° counterclockwise from the vertical, than if the joints are vertical or induced at 14° clockwise from the horizontal. This occurs because the principal stress around that end of the panels rotate so that the normal stresses on the joints inclined at 14° counterclockwise are reduced, while the shear stresses are increased. This effect is quite marked for the lower initial stress state (Figure 11b) since the regions of potential joint activation are extensive. For the higher initial stress state the regions of joint activation are restricted to very shallow depths (Figure 11c and 11d), but the factors of safety against joint activation around the center of the repository are again reduced if the joints are inclined at an angle of 14° counterclockwise from the vertical. Similar changes in the regions of potential joint activation and the calculated factors of safety can also be observed at the outer edge of the repository. Again, these changes can be easily related to the relationship between the joint orientation and the principal stress directions.

4.2 Analyses of Access Ramps

The access ramps, the normal cross section of which is shown in Figure 12, were assumed to be inclined at an angle of 10° to the emplacement horizon (Figure 1). Since the dimensions of the excavation are small in comparison with the length of the ramp, two-dimensional plane strain analyses were utilized. For the analyses the in-plane (x-y plane) stresses for the repository model were calculated for the local coordinate axes x_ℓ and y_ℓ, illustrated in Figure 1. Out-of-plane stresses, in z-direction, were then calculated as described in Section 3.3 The variation of the subsidiary principal stresses σ_z and σ_y^ℓ perpendicular to the longitudinal axis of the ramps is illustrated in Figures 13 (Case 1) and 14 (Case 2). These distributions are for a time 100 years after waste emplacement. Similar variation was observed at 10 and 50 years, except that magnitudes generally were smaller.

Having determined the stress distribution along the assumed path of the access ramps, the HEFF code was used to investigate plane strain behavior of rock in the vicinity of the ramp. For these analyses, the stresses σ_z and σ_y^{ℓ} defined above were assumed to be the total stresses in the plane of the cross-section of the ramp. These stresses were applied as edge loads on a boundary-element model with horizontal and vertical boundaries 20 m from the center of the drift. The shear stresses on the plane of the cross section were ignored, and no account was taken of any rock support that might be installed. The evaluations were carried out for a number of sections along the ramps; specifically, at locations with high mean and high deviatoric stresses. These sample points are listed in Table 1, together with the computed values of the total stress to which the ramp sections would be subjected.

Results of analyses of sections above the panels, where the mean stress is relatively high, are presented in Figures 15 through 19. The potential for either development of new fractures in the rock matrix or the activation of vertical joints parallel to the ramp axis was again considered. The results of the matrix factor of safety calculation are not presented here because the computed values were generally higher than those for joint activation. Instead, the distribution of the tangential stress around the periphery of the openings is presented in Figure 15 and 16. Comparing those boundary stresses with the matrix tensile and compressive strengths of -6.5 MPa and 75.3 MPa, respectively, it is clear that there is little potential for creation of new fractures in the rock matrix even around the opening, which is where any such fracturing would usually be expected to initiate.

From the information presented in Figures 17 and 18 it is clear that high factors of safety against joint activation are predicted throughout the rock mass, except for local areas of activation in the sidewalls of the ramps. In general, those regions of potential activation are so superficial as to appear inconsequential. Only in one case (Figure 17a) is it observed that joint activation might extend more than a few centimeters into the roof of the excavation. That particular case is one for which the low initial stress state was assumed and is associated with modest tension in the roof of the opening. This can be seen in Figure 15a, but its extent into the roof is more clearly illustrated by the plot of the principal stresses around the opening (Figure 19). There is an obvious correlation between the existence of tensile stresses and regions of potential joint activation. This suggests that the joint activation potential is associated with reduction in the normal stress on the joints rather than the development of high shear stresses that might be associated with shear displacements detrimental to the opening stability.

Analyses of cross sections at the end of the ramp, within the shaft pillar, revealed behavior similar to that of midsections. As illustrated in Figures 20 and 21 the stresses around the openings are relatively modest and any region

of potential joint activation is again concentrated in the sidewalls of the opening (Figure 22 and 23).

4.3 Analyses of Shafts

Shaft analyses were completed for two possible locations: one in the center of the repository and the other beyond the outer panel. For both cases, the distance from the center of the shaft to the boundary of the adjacent panel was chosen to be 100 m. That distance is sufficient to avoid very high induced stresses (see Figures 3 and 4). As for the access ramps, two-dimensional analysis was considered appropriate because the vertical extent of a shaft is large in comparison with the diameter. In this case, however, account was taken of the strain out of the plane of the section (i.e., the axial strain) during evaluation of the potential for development of cracks within the liner.

Because the repository scale analyses showed that high stresses are potentially induced in the vicinity of the shafts at later times, analyses were performed for the two alternative shaft sites 100 years after waste emplacement. The distribution of the stress components in the plane of the repository scale model 100 years after waste emplacement is illustrated in Figure 24. From that figure, it is clear that the magnitude of the thermally induced stresses at the inner site is approximately double that at the outer site. In the analyses on which these results are based, it was assumed that there would be a central pillar regardless of the location of the shafts. In fact the central pillar has rather little influence on the state of stress at the outer boundary of the repository, as indicated by the results obtained during the preliminary analyses discussed in Section 3.3. For example, 50 years after waste emplacement in a four-panel repository, the horizontal and vertical induced stresses at a point 100 m from the panel boundary are respectively 1.57 MPa and -1.70 MPa. For the single panel, these stresses are 1.28 MPa and -1.62 MPa.

From Figure 24 it is obvious that the highest stresses occur at the repository horizon. Those stresses and the computed out-of-plane stresses for the repository scale model are listed in Table 2. The table also lists the axial strain, which it is assumed will be transmitted directly to the shaft liner.

To provide a simple means of evaluating the potential effect of the induced stresses listed in Table 2, typical shaft and shaft liner dimensions were selected:

Shaft external diameter	6.5 m
Shaft lining thickness	0.5 m

The material parameters for the rock mass were the same as listed in section 2.2 and the following properties for the concrete liner were assumed:

Elastic modulus	27.6 GPa
Poisson's ratio	0.15
Uniaxial compressive strength	34.5 MPa (5000 psi)
Uniaxial tensile strength	-3 MPa

Here, the uniaxial tensile strength (σ_t) of unreinforced concrete has been estimated from the compressive strength (σ_c) using the relationship (Wastiels, 1979):

$$\sigma_t = -0.28\ \sigma_c^{0.67},$$

where the units of σ_c and σ_t are MPa.

Stress analyses of the shaft liner were performed using the computer code SHAFT, which was described in Section 3. For the purposes of those analyses, it was assumed that the liner would be emplaced after all stress relaxation (elastic recovery) had taken place. The only loads experienced by the liner, which was assumed to be completely bonded to the shaft wall, are therefore the thermally induced axial strains and the stresses due to interaction with the adjacent rock mass. On the other hand, the rock mass experiences both the initial and induced stresses. The results of the liner analyses are summarized in Tables 3 and 4, where maximum and minimum values of the stresses at the inside and outside of the liner are listed for the internal and external shaft locations respectively. Note that no mention is made of the initial stress, because the liner is assumed to experience only the thermally induced stress.

As indicated by the data presented in Tables 3 and 4 the stress state in the concrete liner is insufficient to cause compressive failure. However, there are significant tensile stresses in the vertical direction because of the imposed axial strain. For the case of the shaft in the center of the repository these stresses appear to be sufficiently high for there to be a potential for development of horizontal cracks in the liner.

5. CONCLUSIONS

Thermomechanical analyses of a repository consisting of a number of waste emplacement panels were performed. From the preliminary analyses that are discussed in section 3.3 it was concluded that three-dimensional effects were relatively minor and it was therefore appropriate to analyze the state of stress in the rock mass around a repository assuming two-dimensional plane strain conditions and a simple configuration consisting of four long waste emplacement panels. The results of the stress analyses were used to evaluate the potential for nonlinear behavior of the rock mass and to determine boundary conditions for stability calculations for ramps and shafts.

Using simplified models of the repository and the rock mass constitutive behavior, various potential modes of behavior on the repository scale as well as of the access ramp and the shaft were examined. Potential behavior of the rock mass comprised development of new fracture in intact material, either under compressive or tensile stresses, and activation of joints and any other preexisting planes of weakness. For the waste characteristics and material parameters considered, it was determined that the potential for development of new fractures in the rock mass is low. There is some potential for joint opening near the ground surface above the repository and there could be large regions of potential joint activation above waste panels if the initial horizontal stresses are low. The extent of the joint opening and potential joint activation is associated with a reduction in the horizontal stresses above the repository and is therefore very sensitive to the initial stress state. It will also be influenced by the variations in the rock mass thermomechanical properties with depth, which was not considered in this study.

More detailed analyses of rock mass around access ramps and shafts also confirmed the conclusion that there is little potential for development of new fractures within the rock mass. For ramp access, the results of the large-scale calculations were used to determine the expected stress state in the rock mass, along the path of the ramp. Those stresses were then used as boundary conditions for analysis of the ramp section at several sample points along its path. The results of the analyses indicated that the stresses around the perimeter of the drift are generally compressive and considerably less than the compressive strength of the rock, even where the drift passes relatively close to the waste emplacement panels. Post-processing of the results of the stress analyses revealed very little potential for local nonlinear behavior associated with slip on the assumed set of vertical joints. Accordingly, it is concluded that a moderate separation of the ramps from the nearest waste panel will ensure minimal potential impact on excavation stability.

Analysis of the ramp drift at the point where it meets the repository horizon indicated little cause for concern. However, it should be noted that any ramp would be likely to turn before reaching a central shaft and the access drift may then parallel the boundary of the waste emplacement panels. Stresses experienced at the access drift on the edge of a panel are discussed in another report (St. John, 1987b).

For shaft access, two possible locations were examined using a similar approach to that adopted for access ramps; the results of large-scale studies were used to determine the boundary conditions for more detailed models. The analyses indicated that more severe stress states would be experienced at a shaft in a central pillar, but those stresses appear to be low in comparison to the compressive strength of a typical concrete liner. However, in all cases it was predicted that the lining would be subject to tensile stresses in the vertical direction. These could be sufficiently large to initiate tensile cracks, but

there is no evidence to suggest that such cracking would be detrimental to the performance of a liner. However, the occurrence of thermally induced stresses within the liner should be addressed during the design of the shafts of a repository.

The results of the investigation have tended to reemphasize the importance of the initial stress field in determining the response of the rock mass to the thermal loading imposed upon it by a nuclear waste repository. In particular, the assumption of a low initial horizontal stress leads to the prediction of large regions of potential joint activation above the waste panels. However, it should be observed that joint activation is not necessarily detrimental to the repository performance, since neither joint slip nor joint opening can be construed as mechanical failure of the repository.

6. REFERENCES

Brady, B.H.G., "HEFF. A Boundary-Element Code for Two-Dimensional Thermoelastic Analysis of a Rock Mass Subject to Constant or Decaying Thermal Loading," User's Guide and Manual, RHO-BWI-C-80. Prepared by the University of Minnesota for Rockwell Hanford Operations, Richland, was, June, 1980.

Johnstone, J.K., R. R. Peters, and P.F. Gnirk, "Unit Evaluation at Yucca Mountain, Nevada Test Site: Summary Report and Recommendations," SAND83-0372, Sandia National Laboratories, Albuquerque, NM, 1984.

MacDougall, H. R. (Compiler), "Site Characterization Plan Conceptual Design Report," Draft SAND84-2641, Sandia National Laboratories, Albuquerque, NM, November, 1986.

Nimick, F. B., S. J. Bauer, and J. R. Tillerson, "Recommended Matrix and Rock Mass Bulk, Mechanical, and Thermal Properties for Thermomechanical Stratigraphy of Yucca Mountain," Version 1, Keystone Document Number 6310-85-1, Division 6314, Sandia National Laboratories, Albuquerque, NM, 1984. Contained in Appendix O of the SCP-CDR (SAND84-2641).

Shirley, C. G., "Keystone Memorandum 6310-83-1: Reference Waste Emplacement Geometries," SLTR 83-1001 Sandia National Laboratories, Albuquerque, NM, June, 1983a, Published as Appendix C to SAND84-1153, "Underground Facility Area Requirements for a Radioactive Waste Repository at Yucca Mountain by A. J. Mansure.

Shirley, C. G., "Keystone memorandum 6310-83-2: Reference Commercial Nuclear Waste Thermal Power and Energy Functions," SLTR 83-1002 Sandia National Laboratories, Albuquerque, NM, August, 1983b.

St. John, C. M., "Investigative Study of the Stability of Underground Excavations for a Nuclear Waste Repository in Tuff," SAND83-7451, Sandia National Laboratories, Albuquerque, NM, July, 1987a.

St. John, C. M. , "Thermomechanical Analysis of Underground Excavations in the Vacinity of a Nuclear Waste Isolation Panel" SAND84-7208, Sandia National Laboratories, Albuquerque, NM, June 1987b.

St. John, C. M. and M. Christianson, "STRES3D. A Computer Program for Determining Temperatures, Stresses and Displacements around Single or Arrays of Constant or Exponentially Decaying Heat Sources," User's Guide and Manual, Report RHO-BWI-C-78. Prepared by the University of Minnesota for Rockwell Hanford Operations, Richland, was, September, 1980.

St. John, C. M., and S. J. Mitchell, "Investigation of Excavation Stability in a Finite Repository," SAND86-7011, Sandia National Laboratories, Albuquerque, NM, May, 1987.

St. John, C. M. and D. E. Van Dillen, "An Investigation of the Failure Resistance of Rockbolted Tunnels for Deep Missile Basing," R-8227-5534. Prepared for Defense Nuclear Agency by Agbabian Associates, El Segundo, CA, September, 1983.

Wastiels, J., "Behavior of Concrete Under Multiaxial Stresses - A Review," Cement and Concrete Review, Vol. 9, pp. 35-44, 1970.

Zeuch D. H. and M. J. Eatough "Draft Reference Information Base for the Nevada Nuclear Waste Storage Investigations Project," Sandia National Laboratories, Albuquerque, NM, April, 1986.

TABLE 1

STRESSES AT SELECTED LOCATIONS ALONG THE PATH OF AN ACCESS RAMP

(a) Points Above the Repository Horizon

Case	Time (Yrs)	Point*	x-Coordinate (m)	σ_z (MPa)	σ_y^{ℓ} (MPa)
1	10	A	140	1.697	5.948
	50	B	160	6.371	7.035
	100	C	200	8.983	8.238
2	10	A	140	6.338	6.088
	50	B	160	10.990	7.174
	100	C	200	13.558	7.376

(b) The Point Where the Ramp Enters a Central Shaft Pillar

Case	Time (Yrs)	Point*	x-Coordinate (m)	σ_z (MPa)	σ_y^{ℓ} (MPa)
1	10	D	-100	2.171	3.895
	50	D	-100	5.475	3.339
	100	D	-100	6.607	3.582
2	10	D	-100	7.073	4.042
	50	D	-100	10.377	3.487
	100	D	-100	11.508	3.730

*See Figure 1

TABLE 2

STRESSES EXPERIENCED AT THE LOCATION OF A SHAFT EITHER IN A 200 m CENTRAL PILLAR OR 100 m FROM THE WASTE PANELS

Shaft Site	Case	Induced Vertical Stress (MPa) (σ_y)	Induced Horizontal Stresses (MPa) In-Plane (σ_x)*	Out-of-Plane (σ_z)	Induced Vertical Strain (ϵ_y)
Inside	1	-4.318	3.851	0.379	$-0.342 * 10^{-3}$
	2	-4.318	3.851	0.379	$-0.342 * 10^{-3}$
Outside	1	-2.118	2.144	0.241	$-0.172 * 10^{-3}$
	2	-2.118	2.144	0.241	$-0.172 * 10^{-3}$

*The induced vertical stress and in-plane horizontal stress for the two-dimensional repository model are illustrated in Figure 24.

TABLE 3

LINER STRESSES FOR A SHAFT LOCATED IN THE CENTER OF A 200 m SHAFT PILLAR

STRESS	Angle (θ) relative to direction of in-plane horizontal stress σ_x			
	θ=0°		θ=90°	
	Inner Fiber	Outer Fiber	Inner Fiber	Outer Fiber
Radial Stress (MPa)	-0.00	0.20	0.0	1.79
Hoop Stress (MPa)	-3.29	0.21	17.31	11.82
Axial Stress (MPa)	-9.93	-9.38	-6.84	-7.40

TABLE 4

LINER STRESSES FOR A SHAFT LOCATED 100m BEYOND THE WASTE PANELS

STRESS	Angle (θ) relative to direction of in-plane horizontal stress σ_x			
	θ=0°		θ=90°	
	Inner Fiber	Outer Fiber	Inner Fiber	Outer Fiber
Radial Stress (MPa)	0.00	0.12	0.0	0.99
Hoop Stress (MPa)	-1.72	0.19	9.57	6.55
Axial Stress (MPa)	-5.00	-4.70	-3.31	-3.62

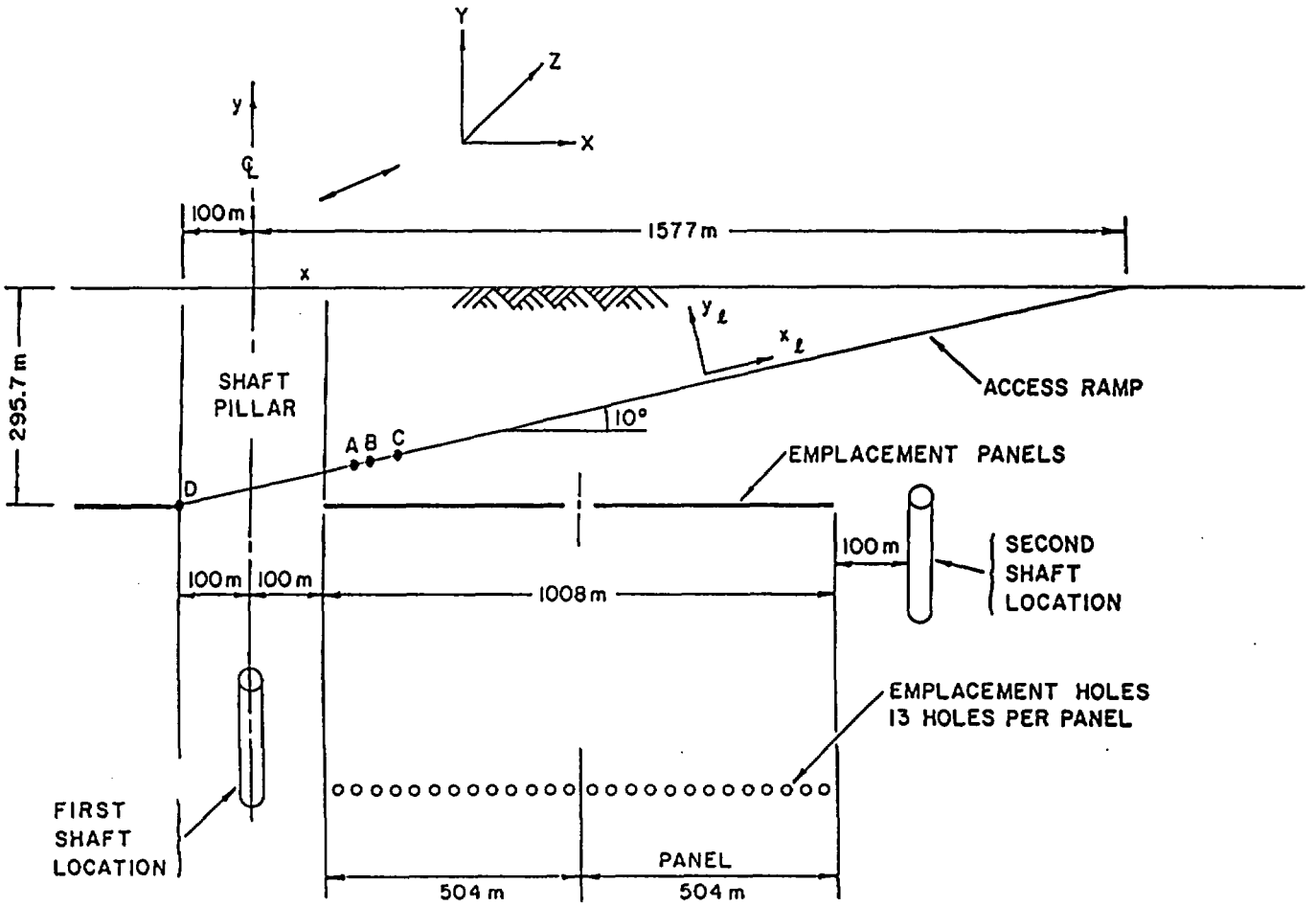

Location of Sample
Points on Access Ramps
A - x = 140.m
B - x = 160.m
C - x = 200.m
D - x =-100.m

Figure 1. Schematic Layout of Panels and Structures

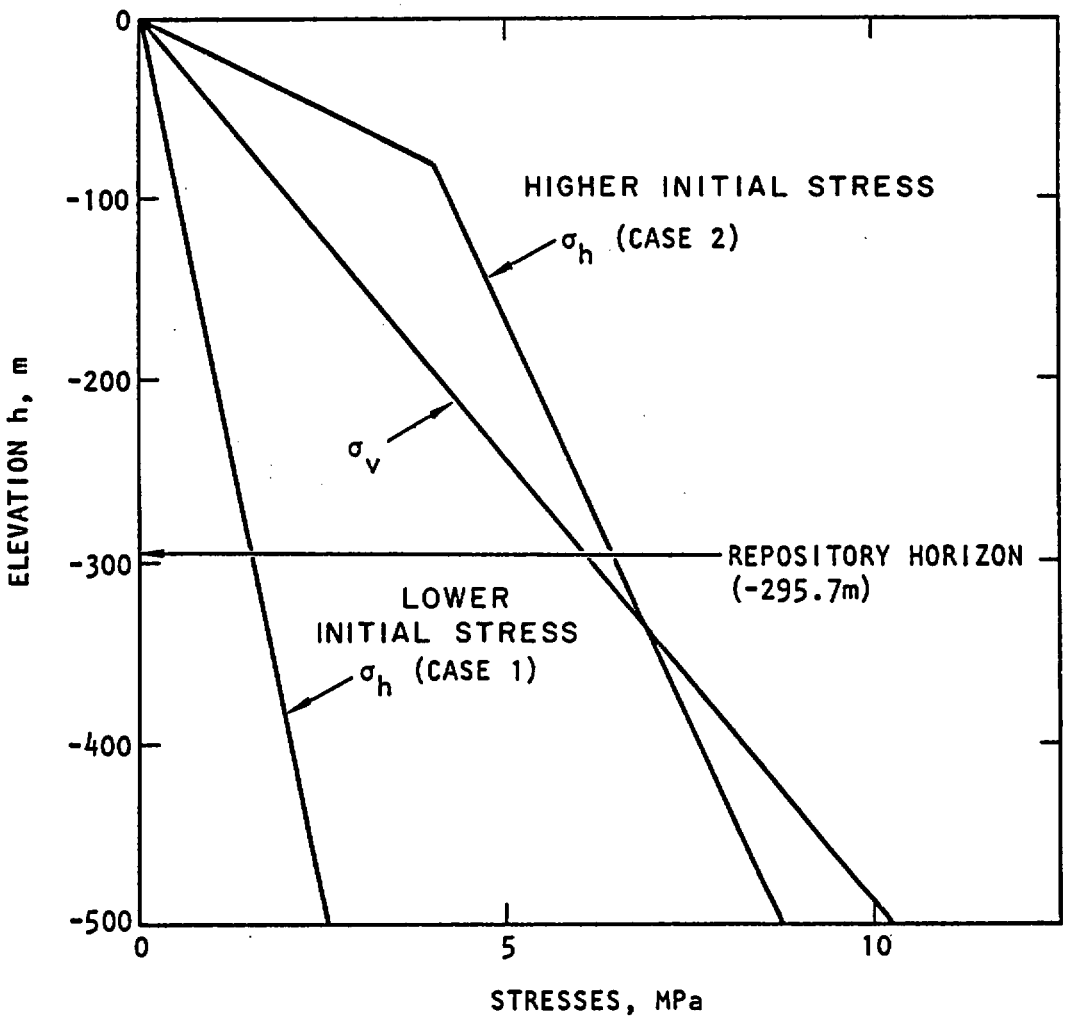

Figure 2. Variation of Vertical and Horizontal Initial Stresses with Depth

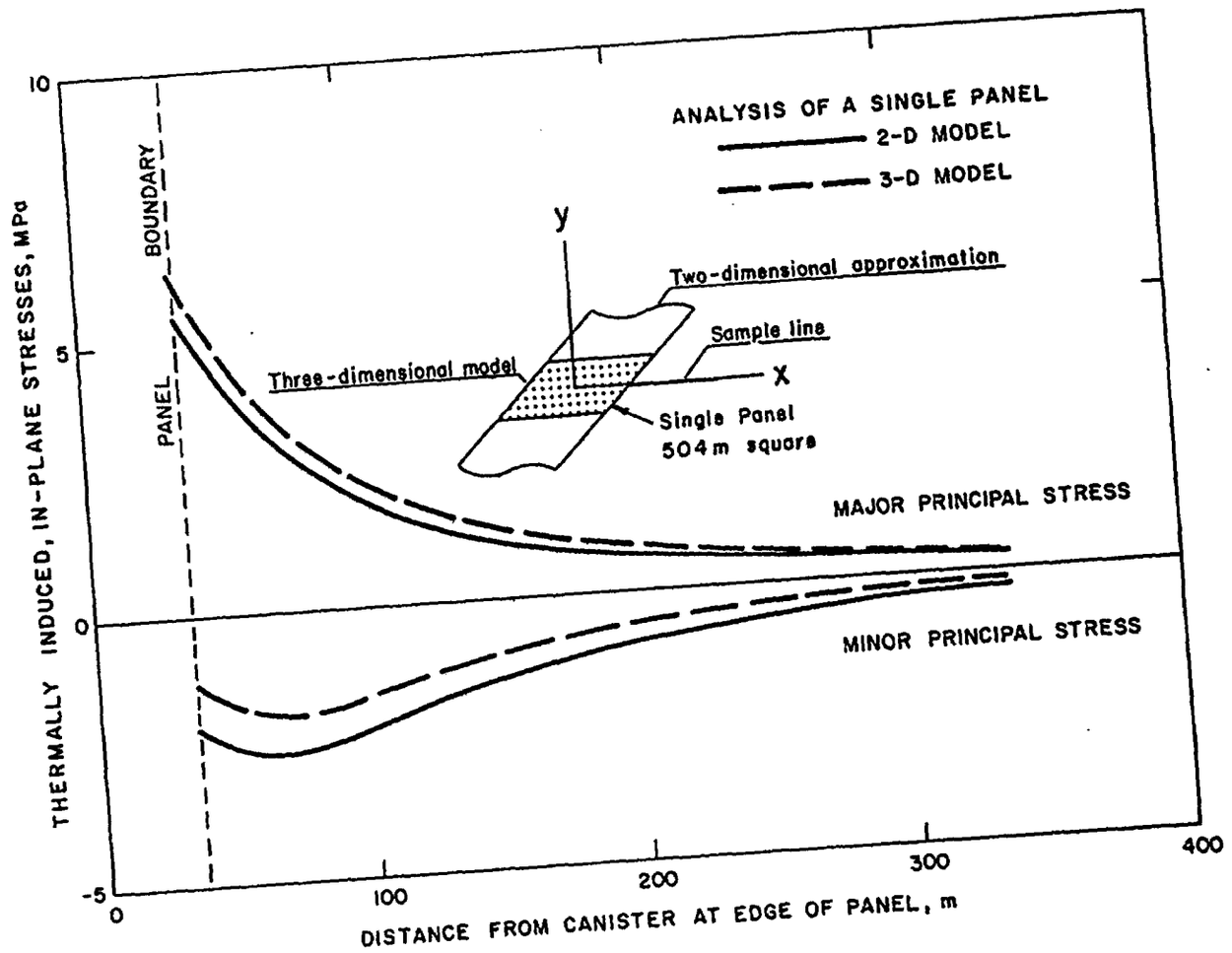

Figure 3. In-Plane Principal Stresses along the Panel Horizon Calculated from Two- and Three-Dimensional Analyses

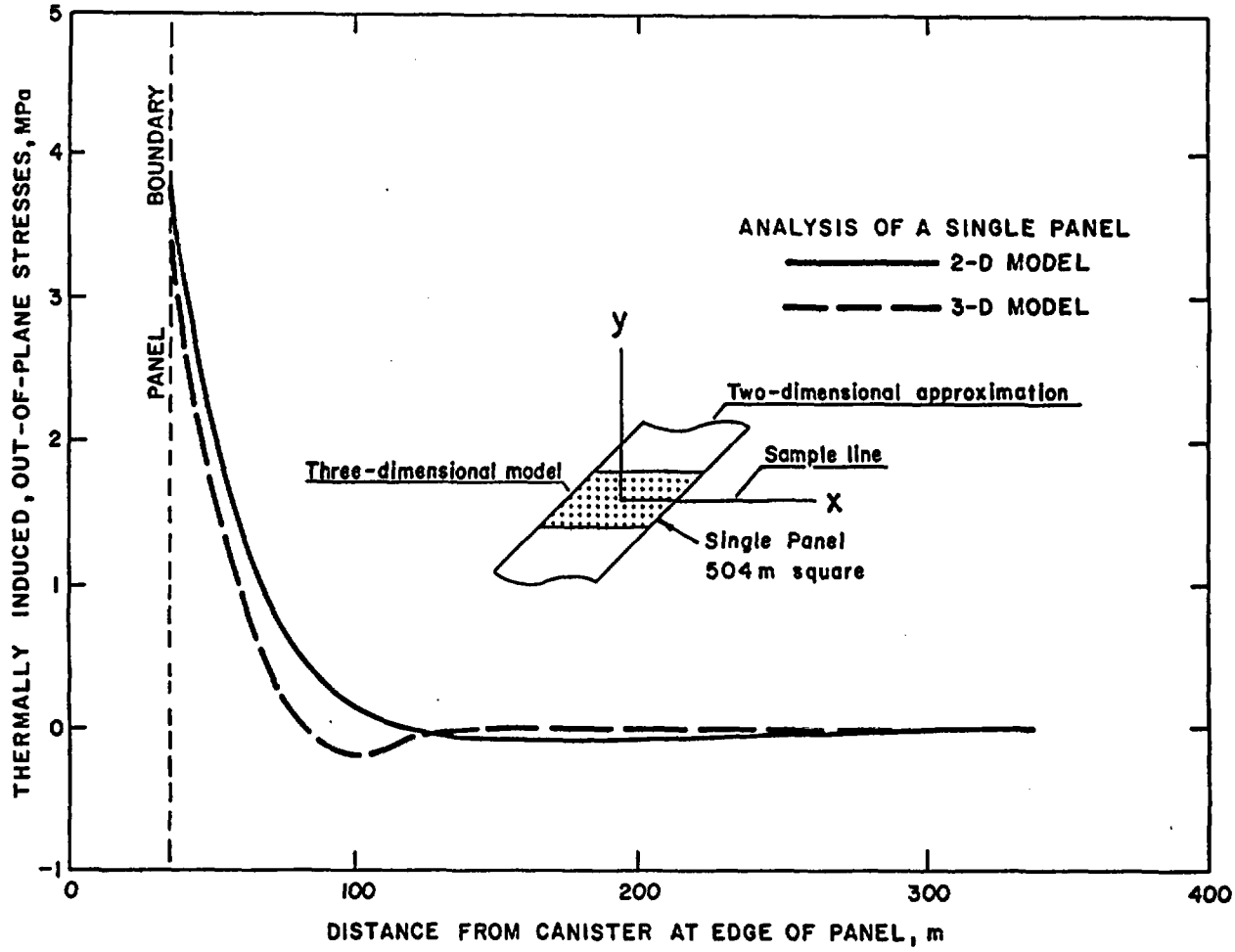

Figure 4. Out-of-Plane Stresses along the Panel Horizon Calculated from Two- and Three-Dimensional Analyses

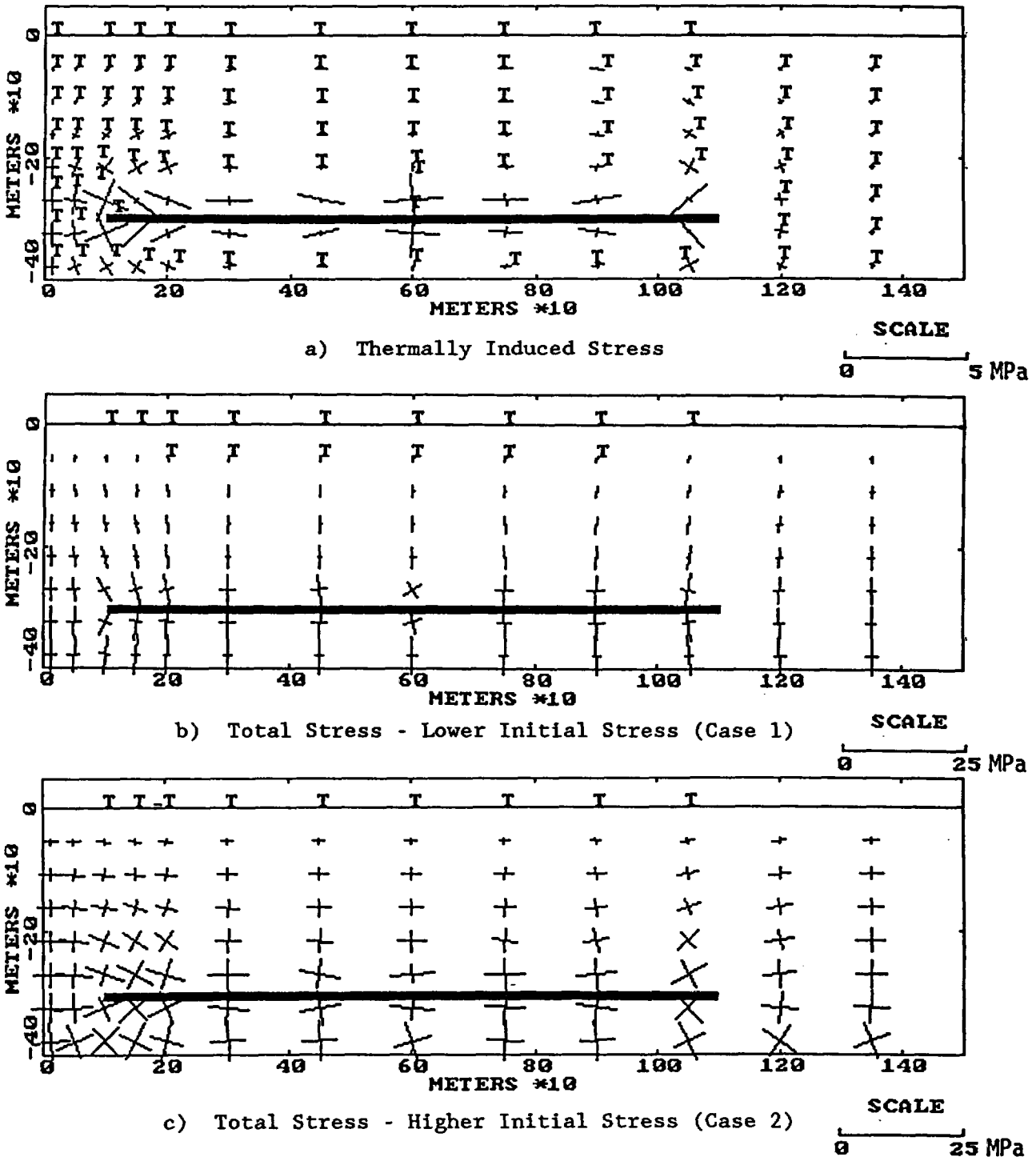

Figure 5. Principal Stresses Due to Thermal Loading in Rock Medium 10 years after Emplacement

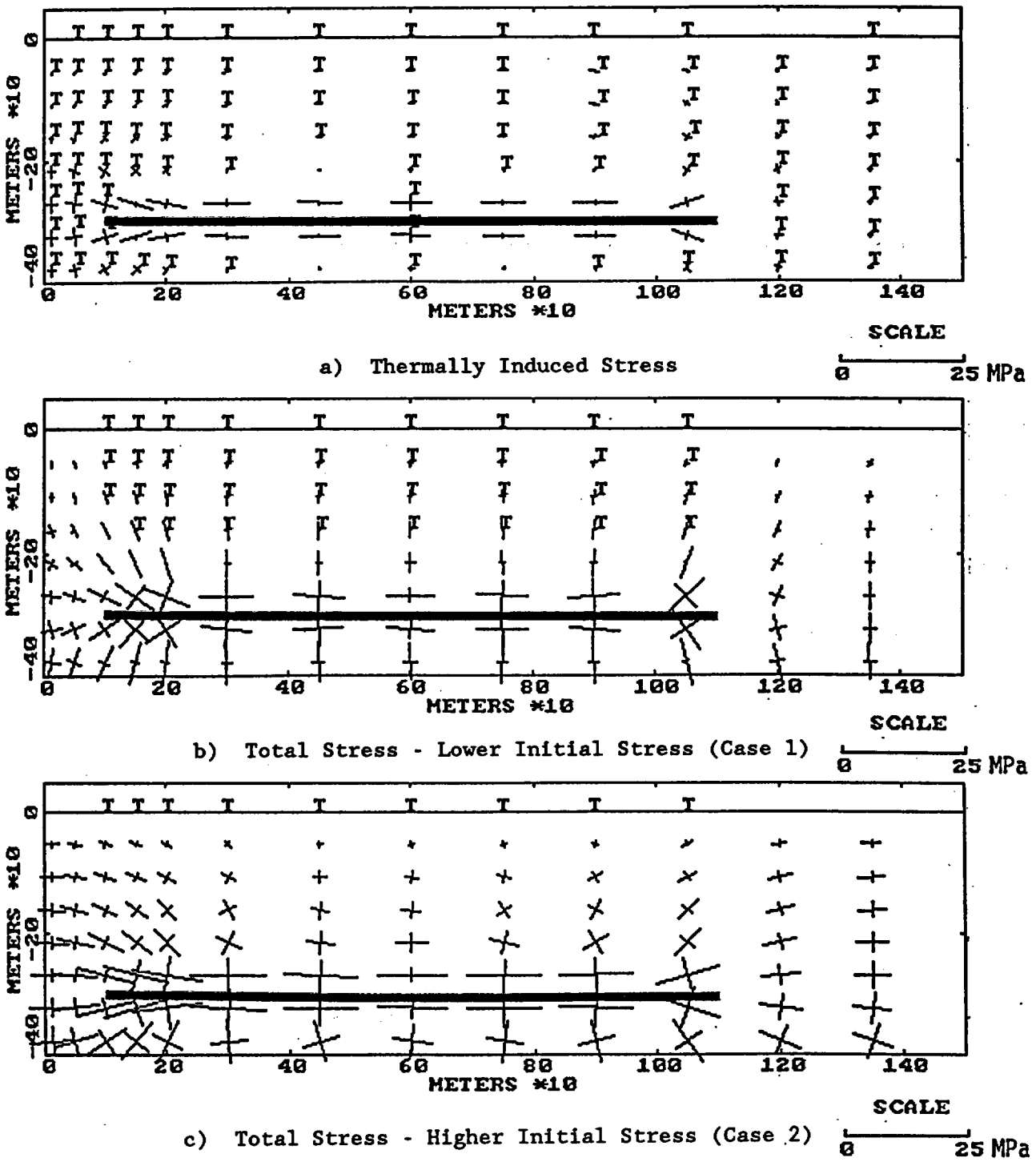

Figure 6. Principal Stresses Due to Thermal Loading in Rock Medium 50 years after Emplacement

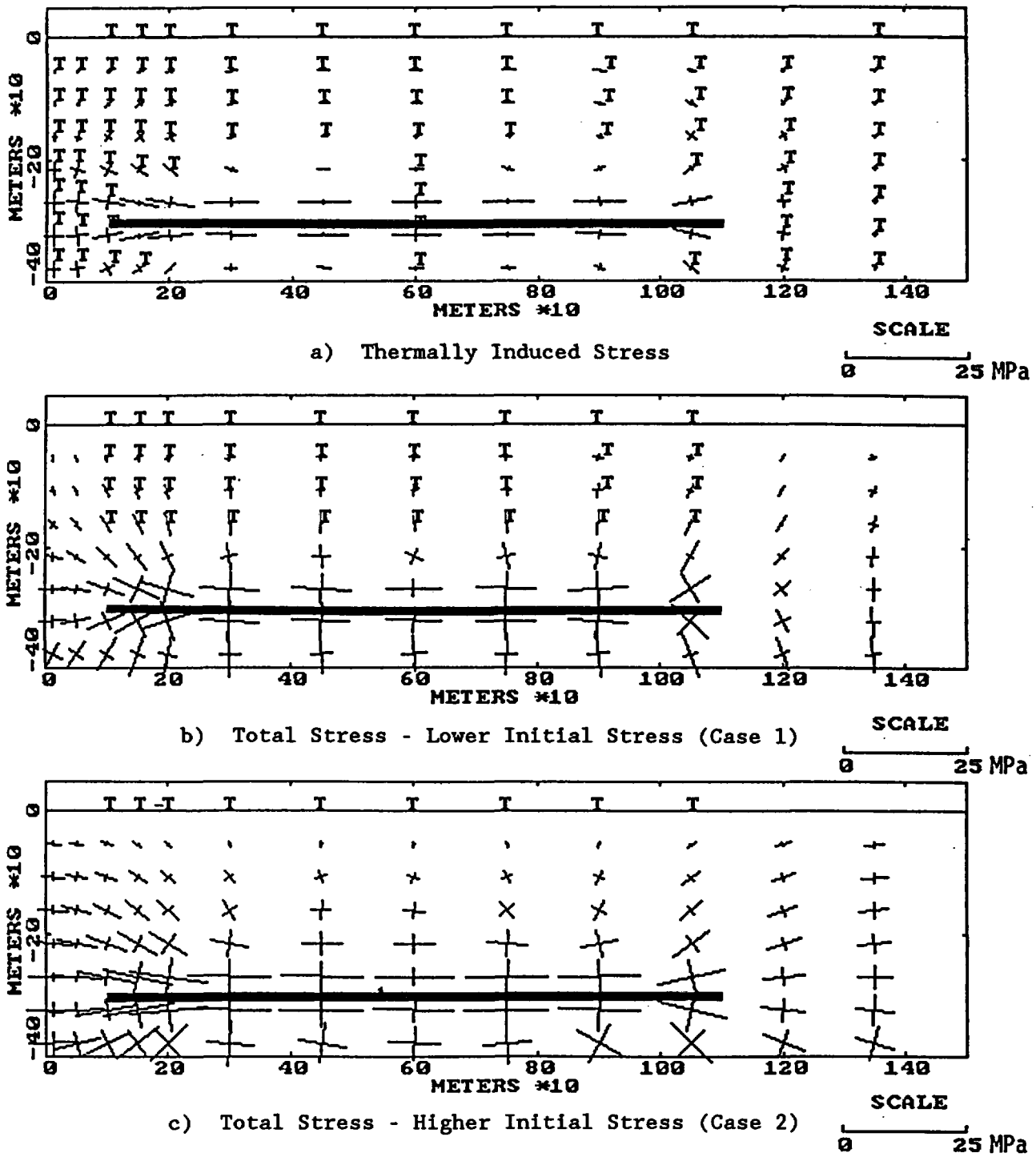

a) Thermally Induced Stress

b) Total Stress - Lower Initial Stress (Case 1)

c) Total Stress - Higher Initial Stress (Case 2)

Figure 7. Principal Stresses Due to Thermal Loading in Rock Medium 100 years after Emplacement

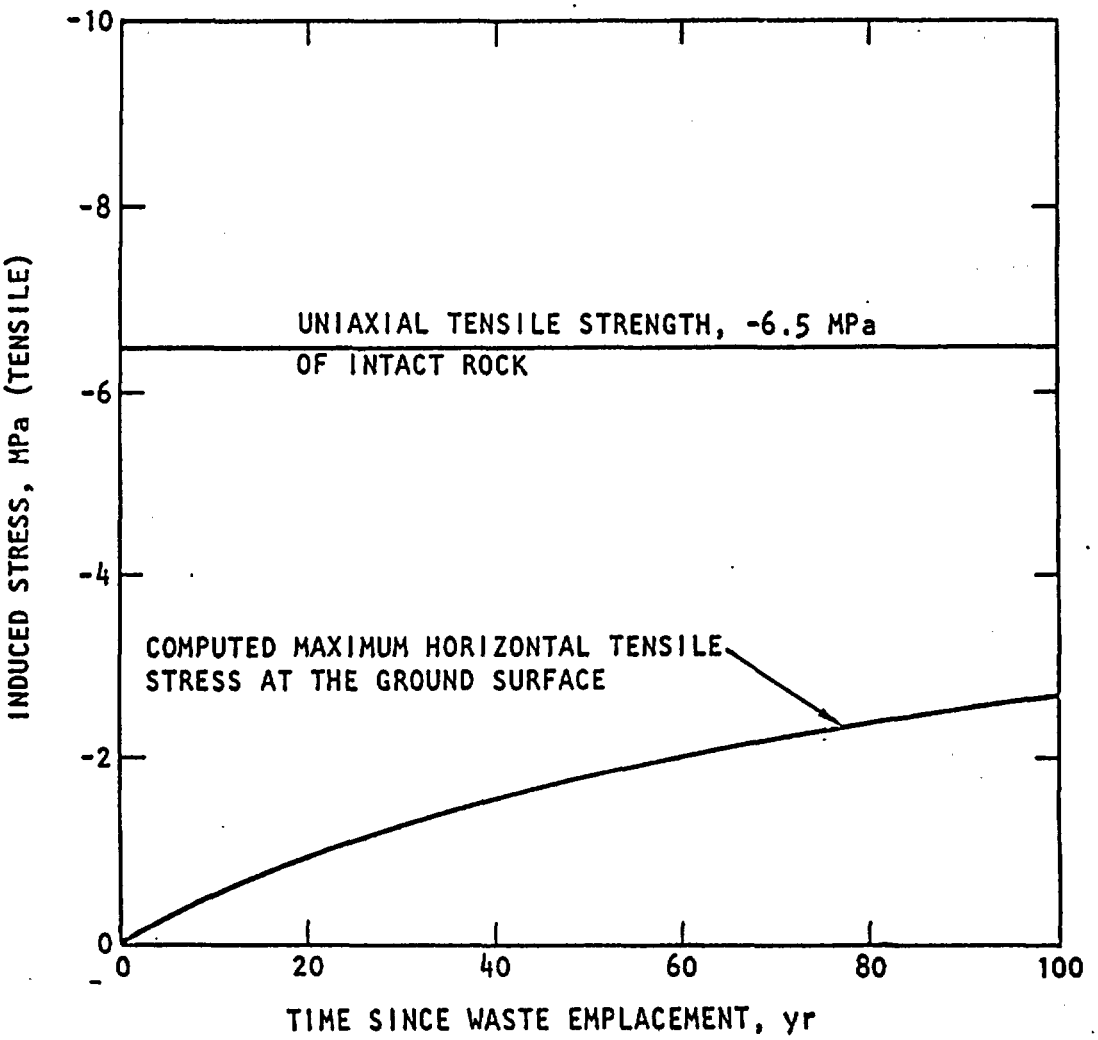

Figure 8. Time Variation of Maximum Tensile Stress at the Ground Surface above a Repository

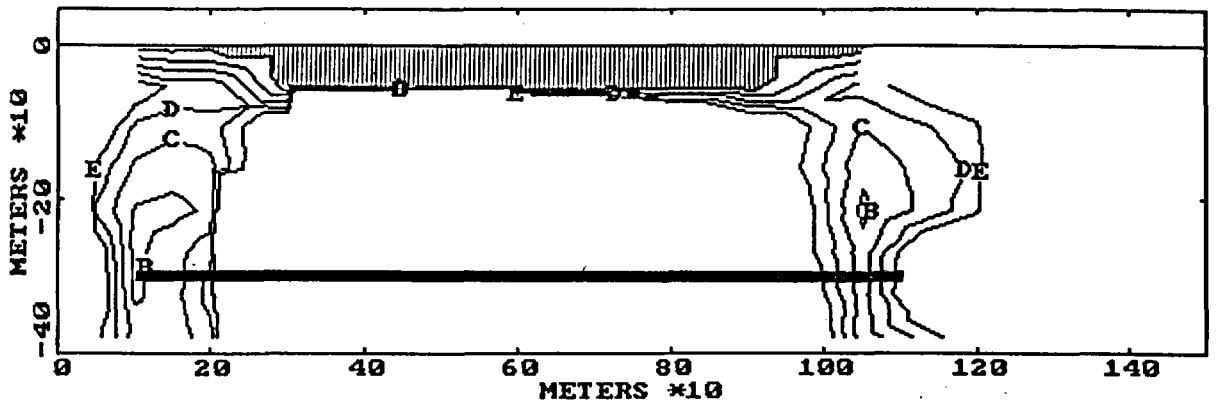

a) 10 Years After Waste Emplacement

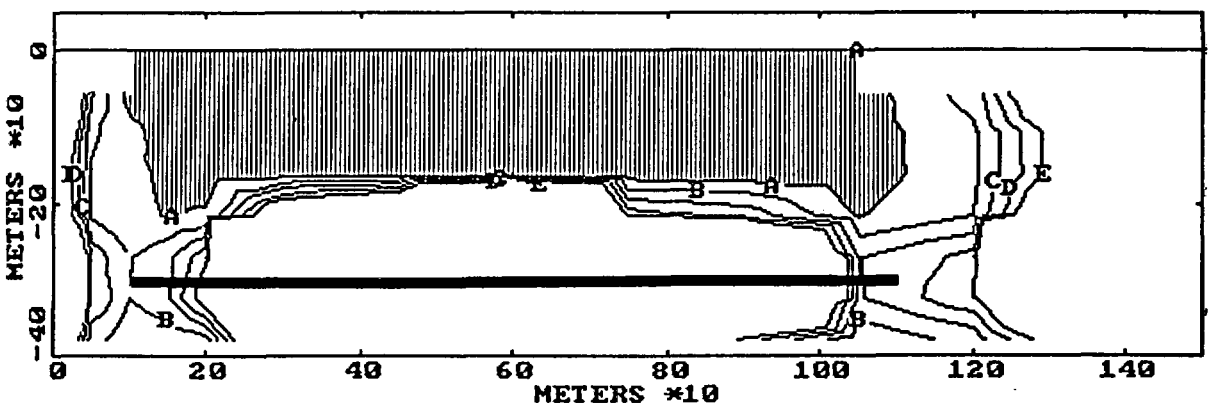

b) 50 Years After Waste Emplacement

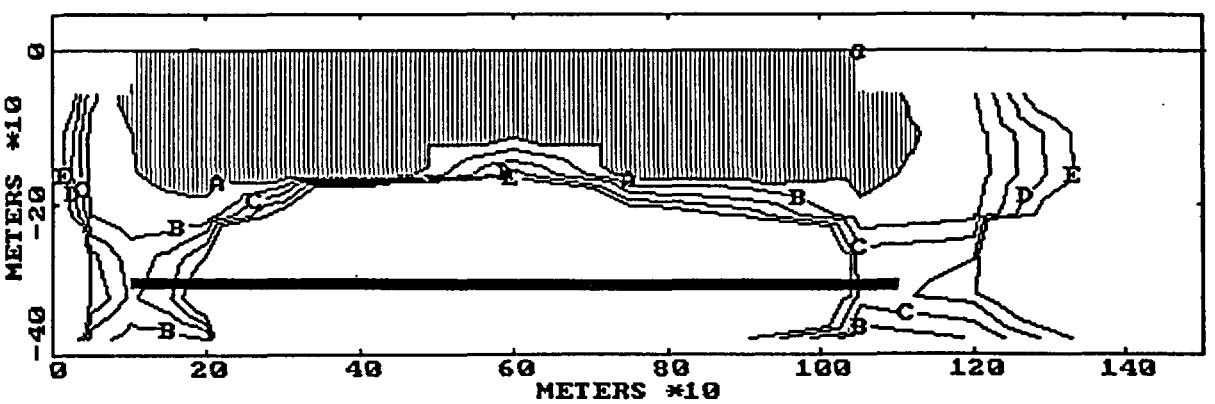

c) 100 Years After Waste Emplacement

Figure 9. Joint Activation Evaluation for the Lower Initial Stress State (Case 1) and Vertical Joints. The Region of Potential Activation is Shaded and the Contour Values are to be Interpreted as: A-1.0, B-3.0, C-5.0, D-7.0, E-9.0

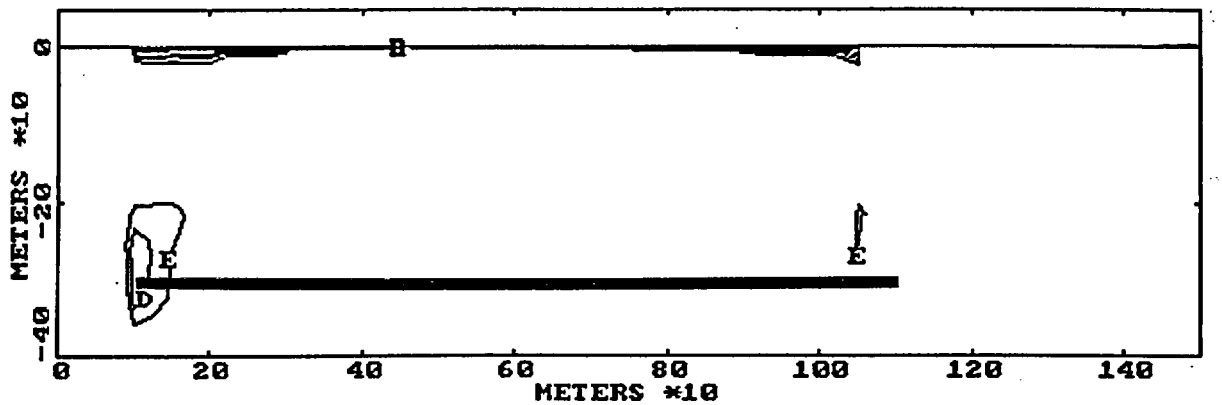

a) 10 Years After Waste Emplacement

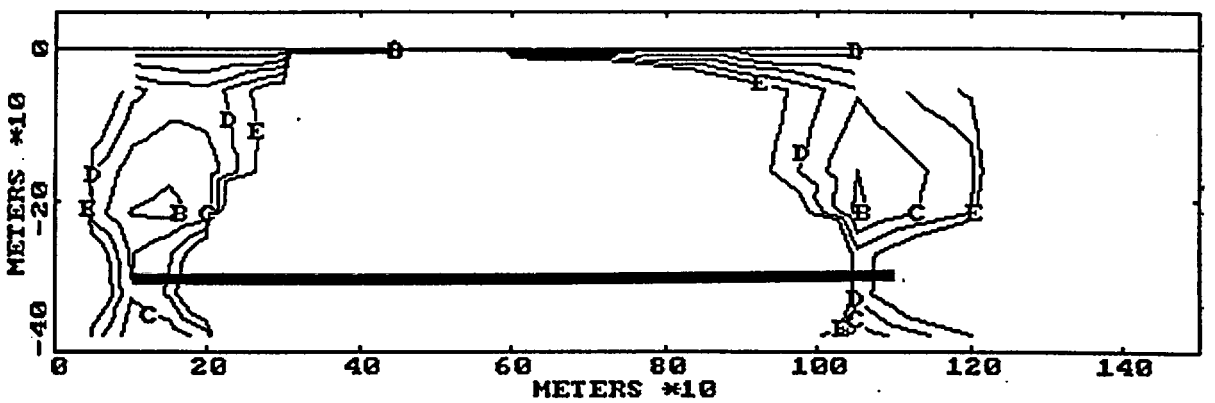

b) 50 Years After Waste Emplacement

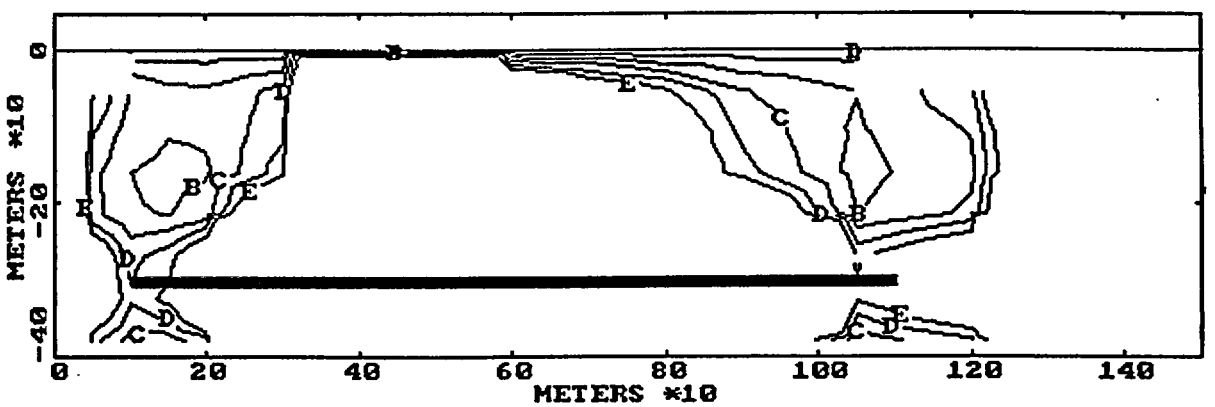

c) 100 Years After Waste Emplacement

Figure 10. Joint Activation Evaluation for the Higher Initial Stress State (Case 2) and Vertical Joints. The Region of Potential Activation is Shaded and the Contour Values are to be Interpreted as: A-1.0, B-3.0, C-5.0, D-7.0, E-9.0

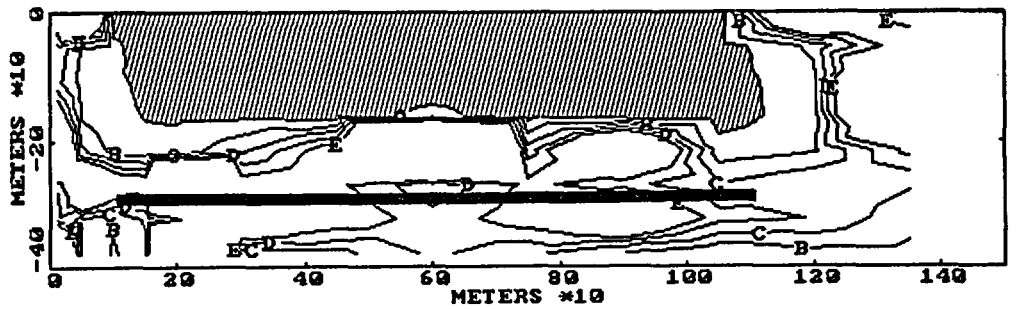

a) Case 1, After 100 Years with Joints at -14°

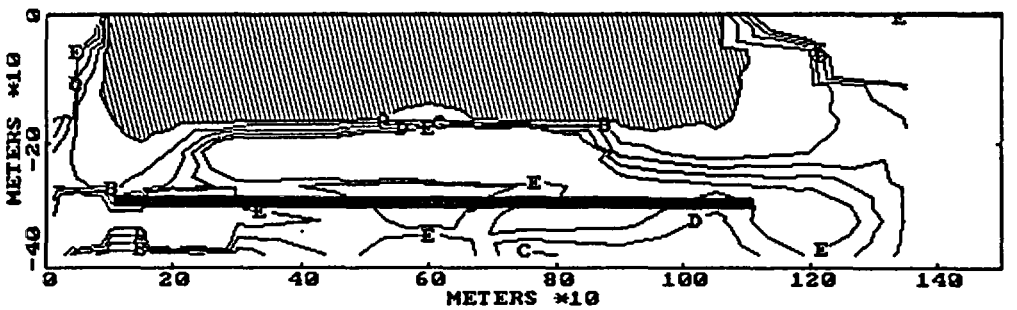

b) Case 1, After 100 Years with Joints at +14°

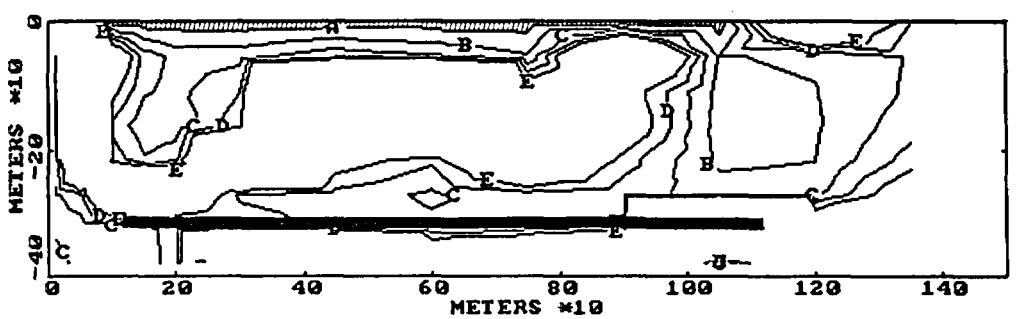

c) Case 2, After 100 Years with Joints at -14°

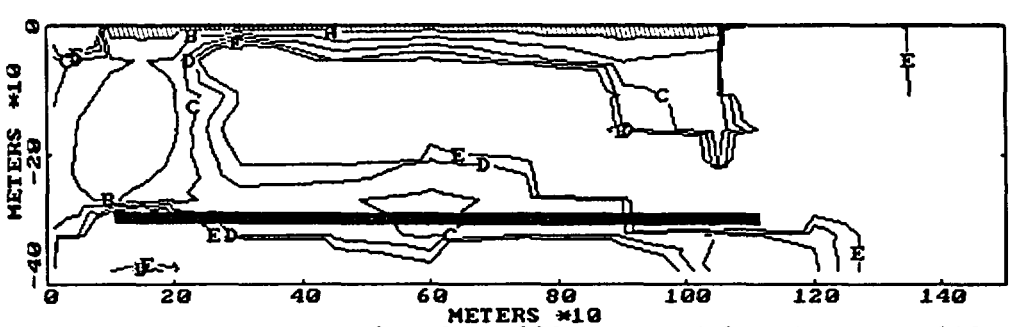

d) Case 2, After 100 Years with Joints at +14°

Figure 11. Joint Activation Evaluation for Joints Inclined at ±14° to the Vertical. The Region of Potential Activation is Shaded and the Contour Values are to be Interpreted as: A-1.0, B-3.0, C-5.0, D-7.0, E-9.0

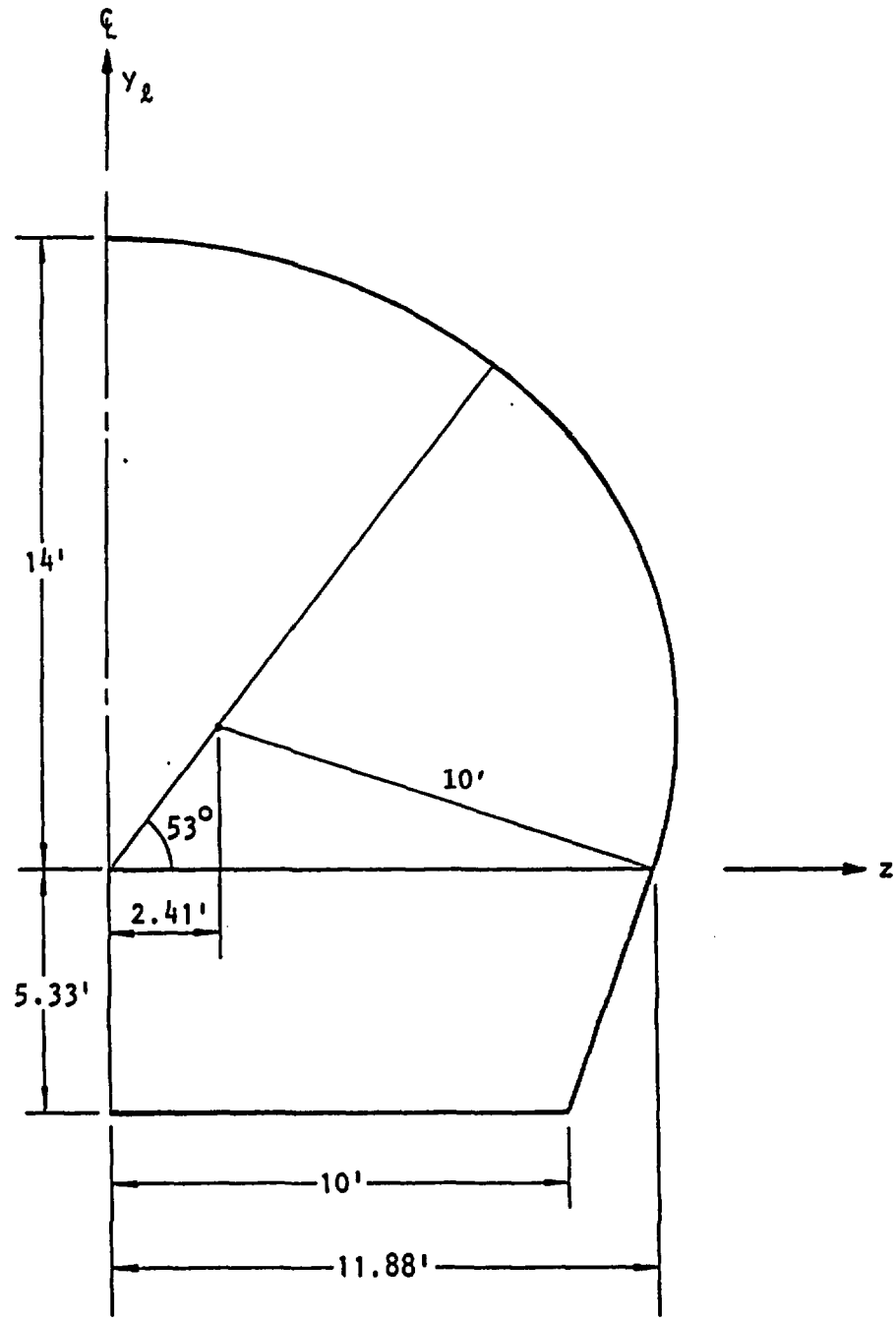

Figure 12. Cross Section of the Access Ramp

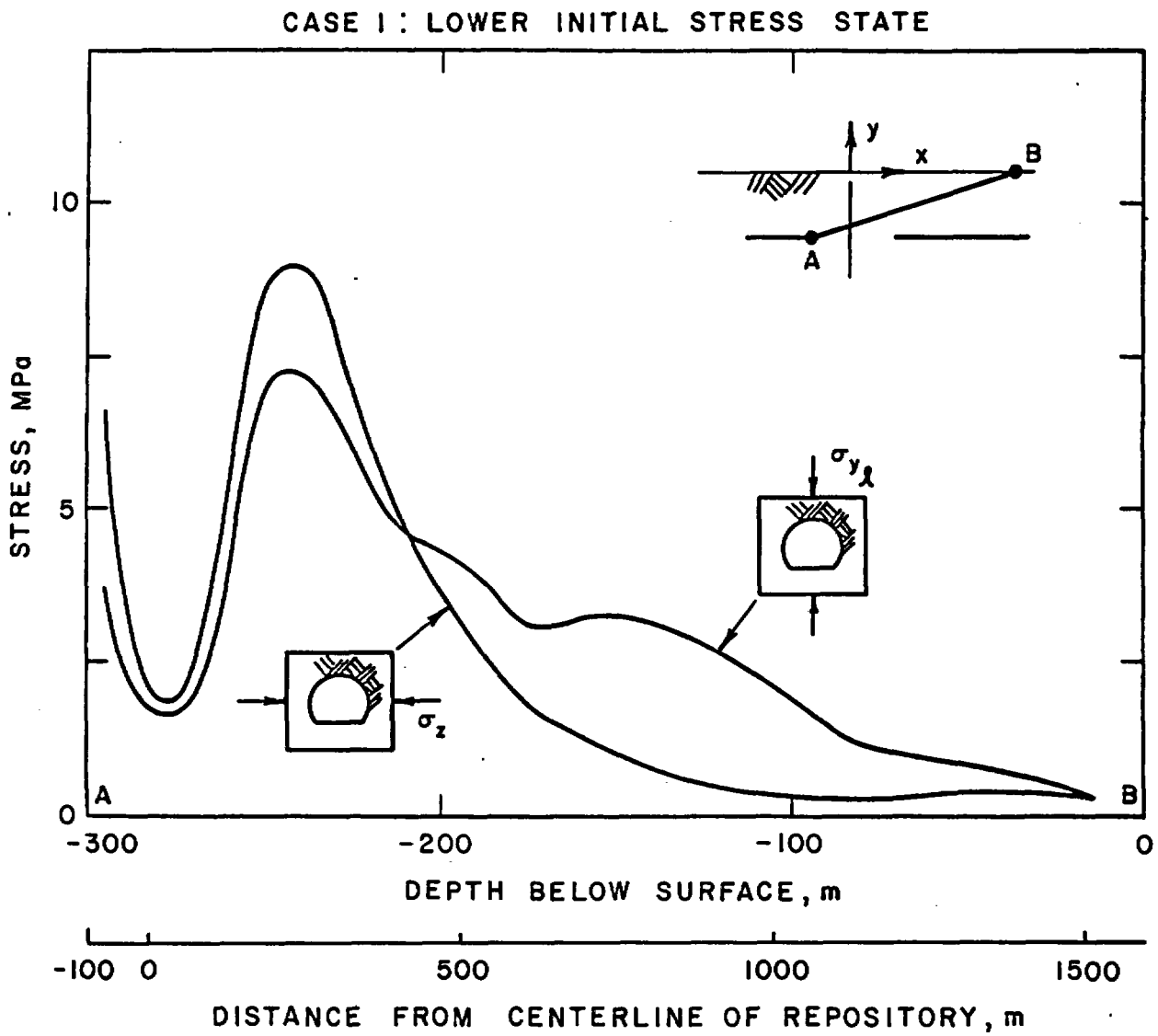

Figure 13. Stress Variation along the Assumed Path of the Access Ramps - for the Lower Initial Stress State (Case 1) - 100 years after Waste Emplacement

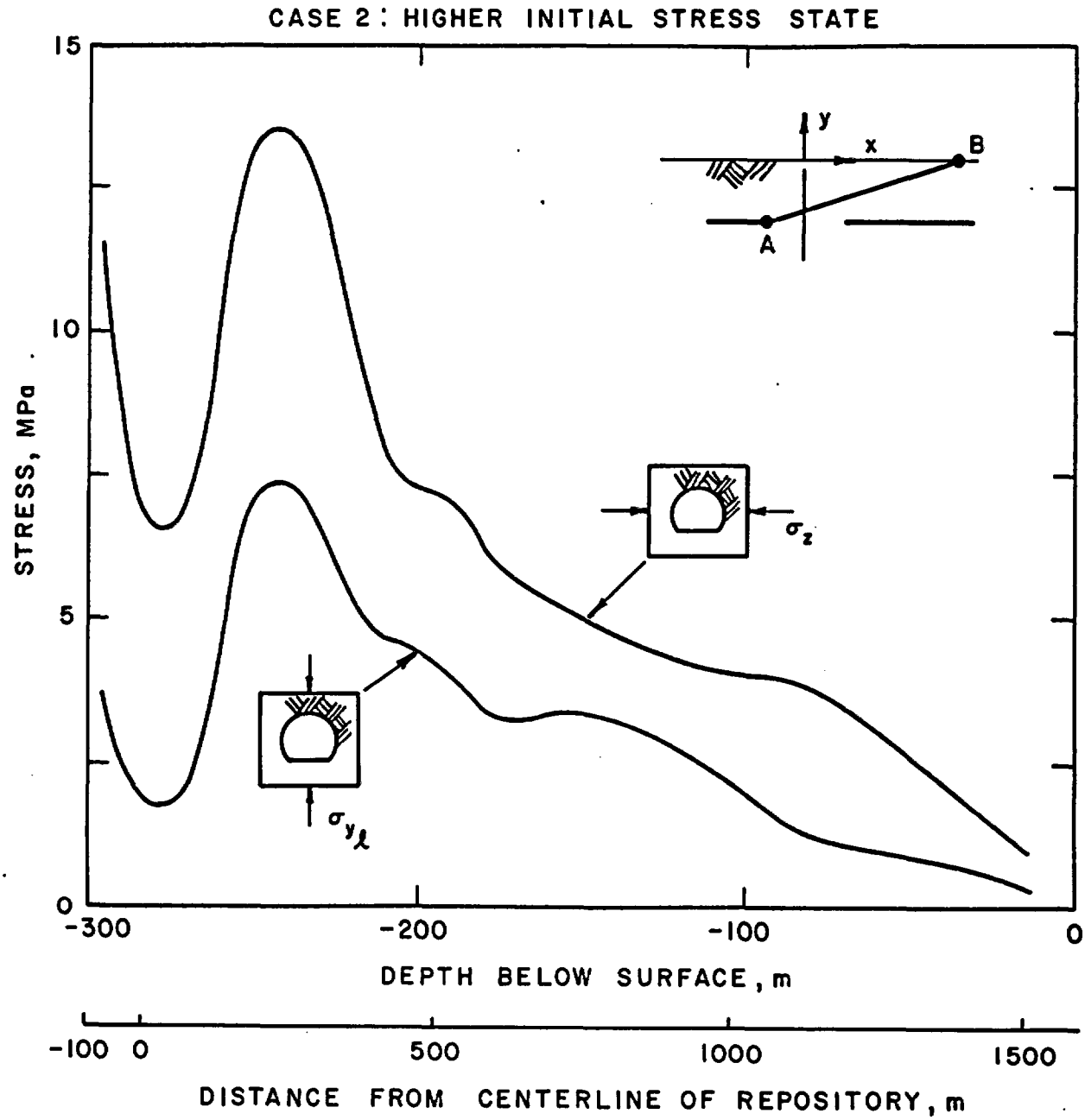

Figure 14. Stress Variation Along the Assumed Path of the Access Ramps - for the Higher Initial Stress State (Case 2) - 100 years after Waste Emplacement

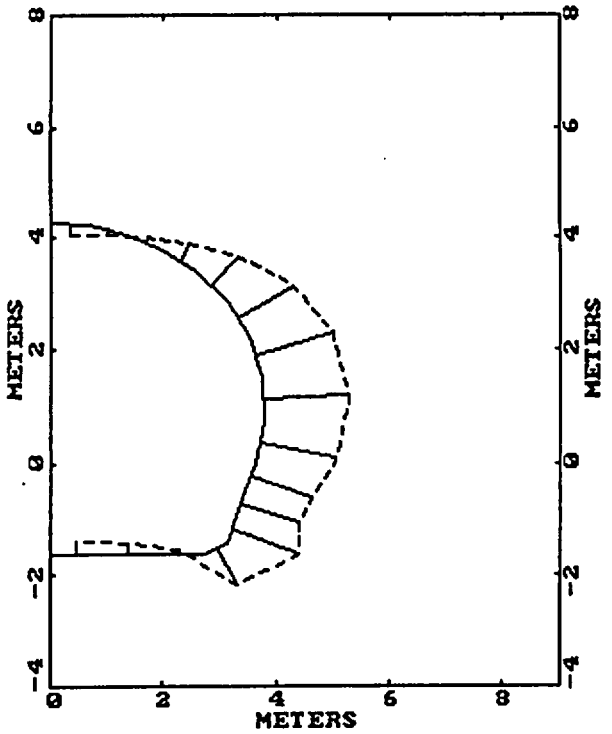

a) Case 1 after 10 yrs at x=140 m

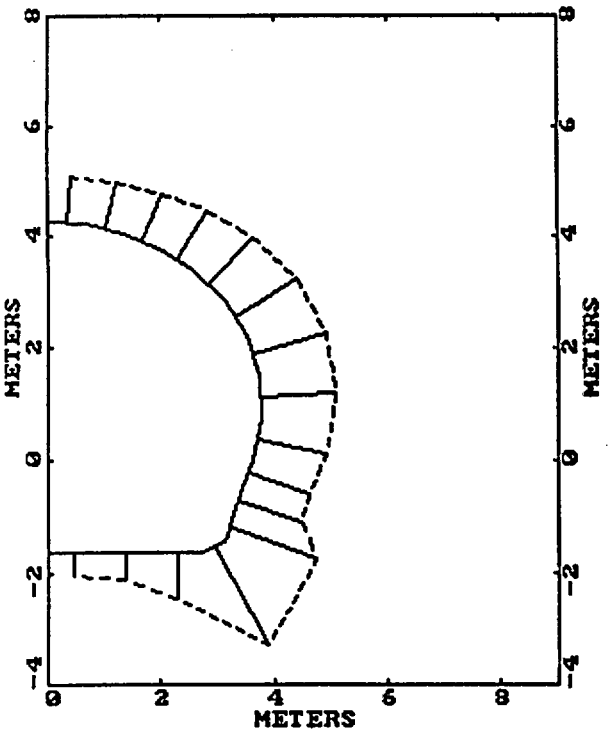

b) Case 1 after 50 yrs at x=160 m

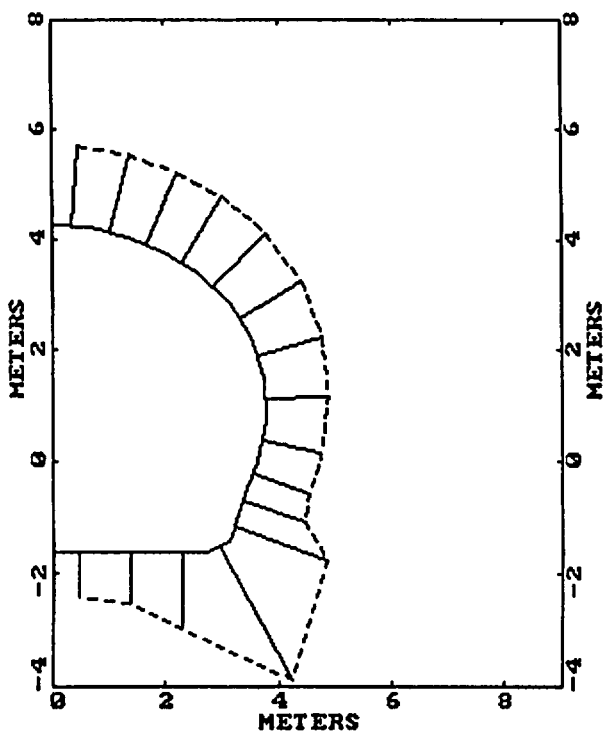

c) Case 1 after 10 yrs at x=200 m

Tangential Stress

30 MPa

Note that a vector pointing out of the opening indicates a compressive stress.

Figure 15. Variation of the Tangential Stress Around the Boundary of the Access Ramp, with the Lower Initial Stress State (Case 1)

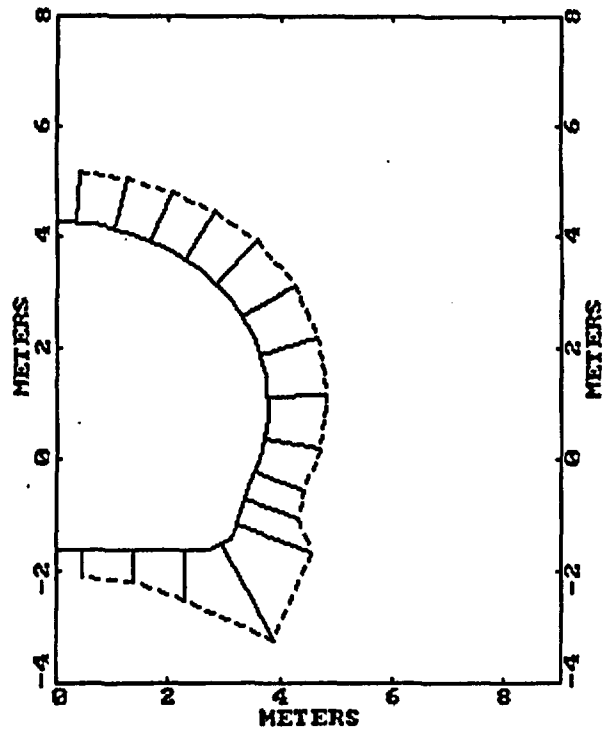

a) Case 2 after 10 yrs at x=140 m

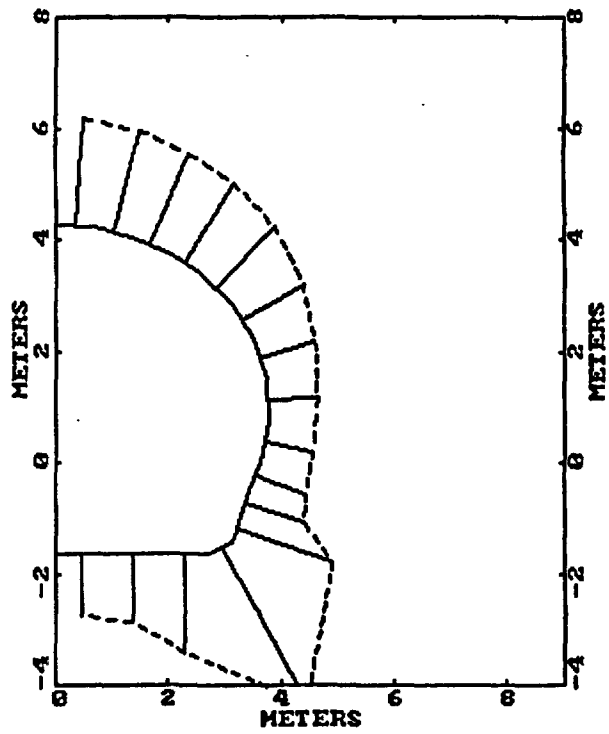

b) Case 2 after 50 yrs at x=160 m

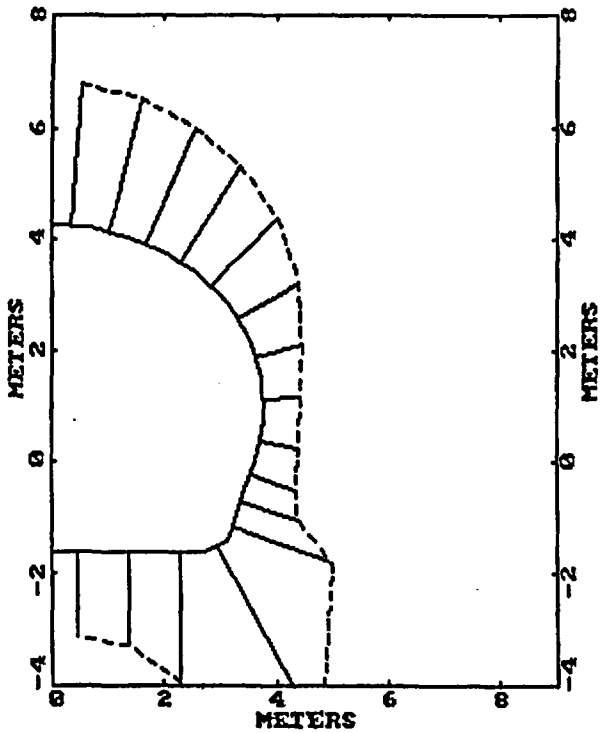

c) Case 2 after 10 yrs at x=200 m

Tangential Stress

30 MPa

Note that a vector pointing out of the opening indicates a compressive stress.

Figure 16. Variation of the Tangential Stress Around the Boundary of the Access Ramp, with the Higher Initial Stress State (Case 2)

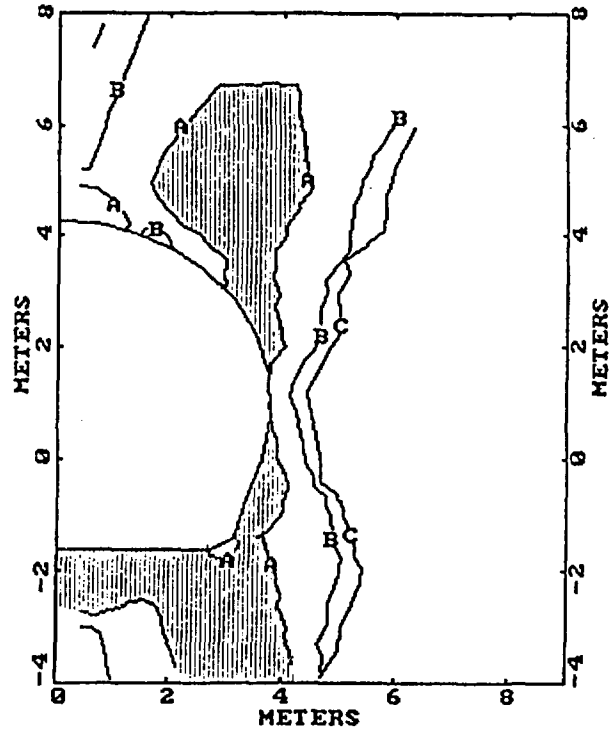

a) Case 1 after 10 yrs at x=140 m

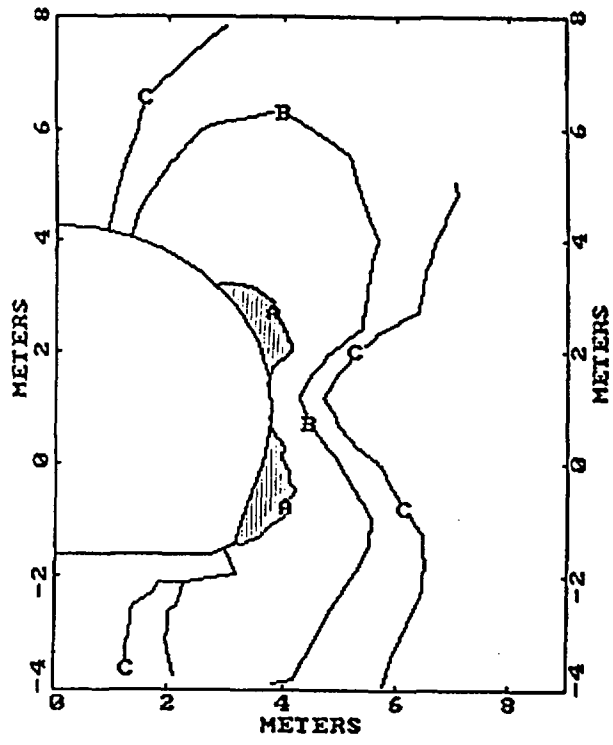

b) Case 1 after 50 Yrs at x=160 m

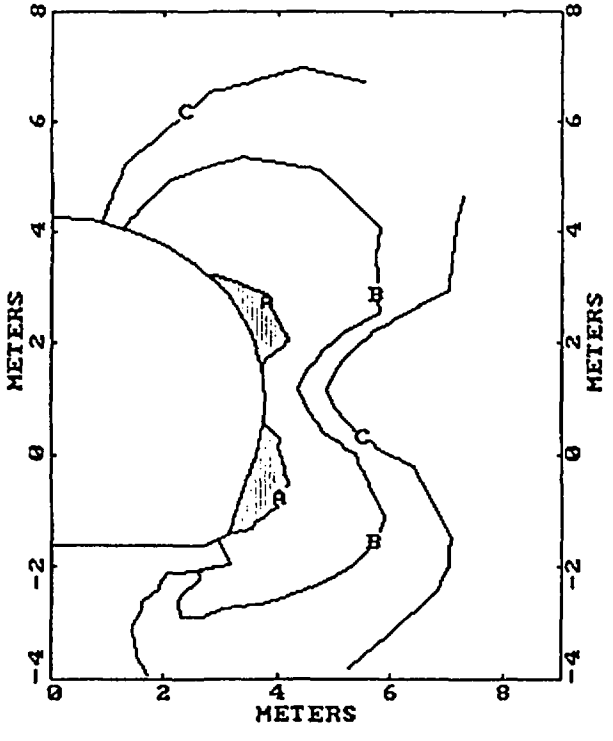

c) Case 2 after 10 yrs at x=200 m

Ratio of Joint Shear
Strength to Shear Stress

A - 1.0
B - 3.0
C - 5.0

Potential Joint
Activation

Figure 17. Joint Activation Evaluation for the Access Ramp for the Lower Initial Stress State (Case 2) and Vertical Joints

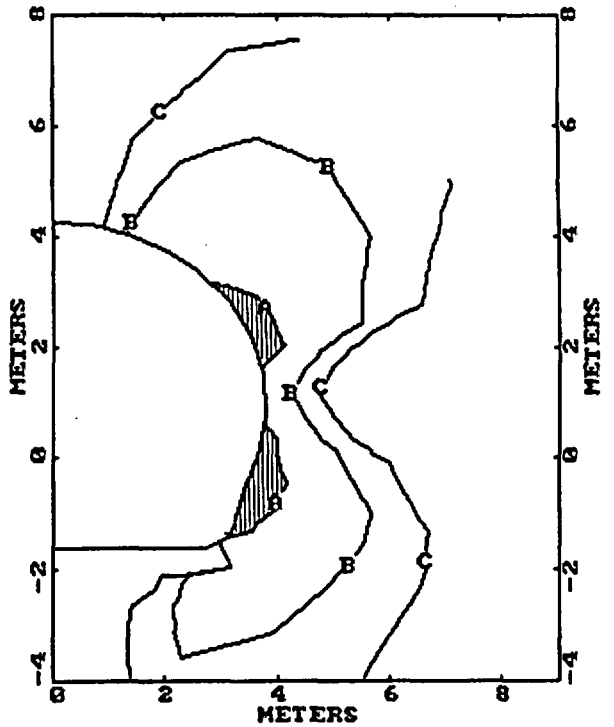

a) Case 2 after 10 yrs at x=140 m

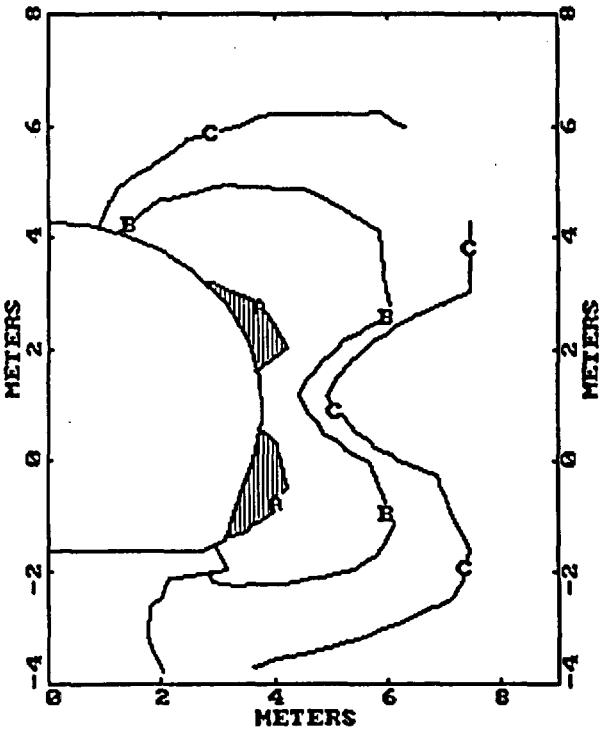

b) Case 2 after 50 yrs at x=160 m

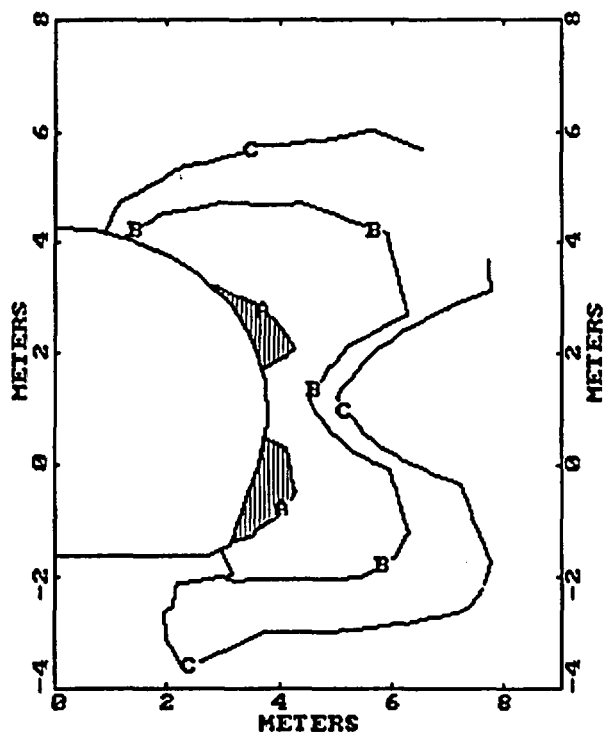

c) Case 2 After 10 Yrs at x=200 m

Ratio of Joint Shear
Strength to Shear Stress

A - 1.0
B - 3.0
C - 5.0

Potential Joint
Activation

Figure 18. Joint Activation Evaluation for the Access Ramp for the Higher Initial Stress State (Case 2) and Vertical Joints

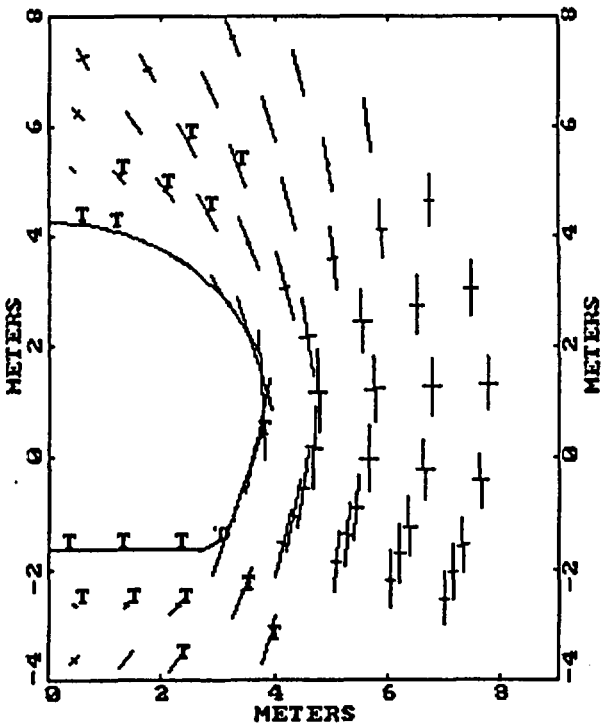

a) Case 1 after 10 yrs at x=140 m

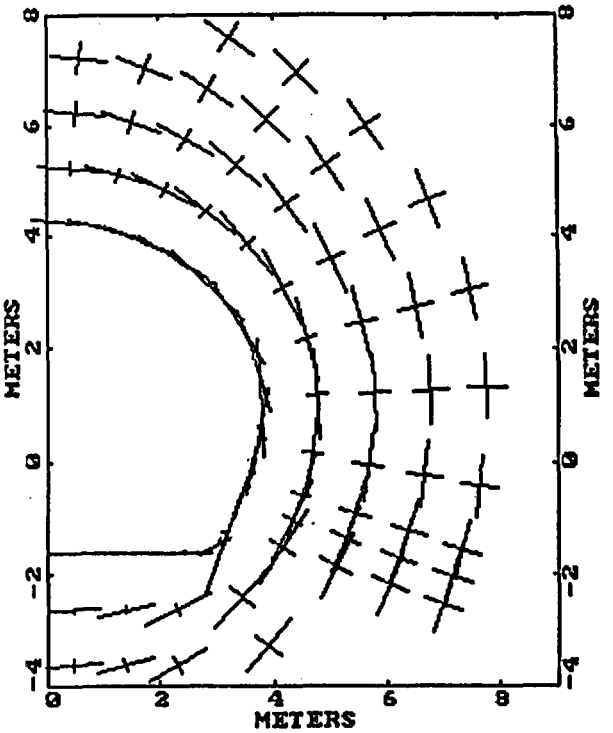

b) Case 1 after 50 yrs at x=160 m

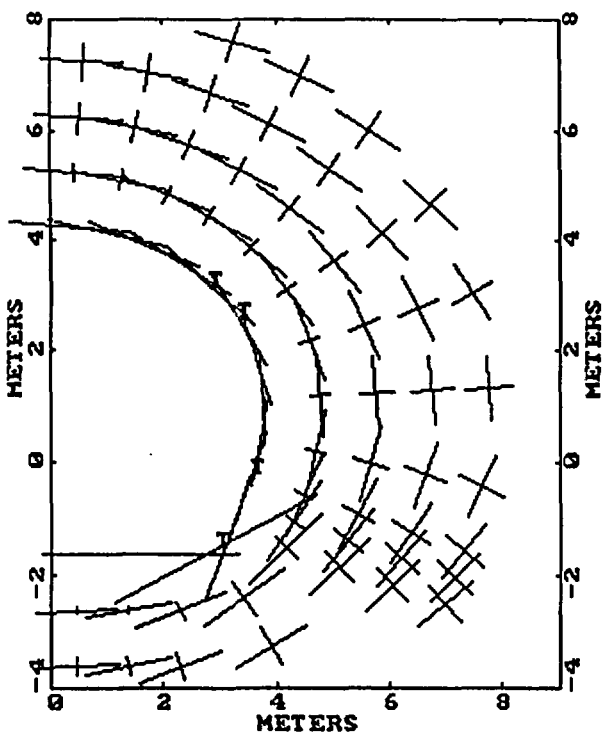

c) Case 1 after 10 yrs at x=200 m

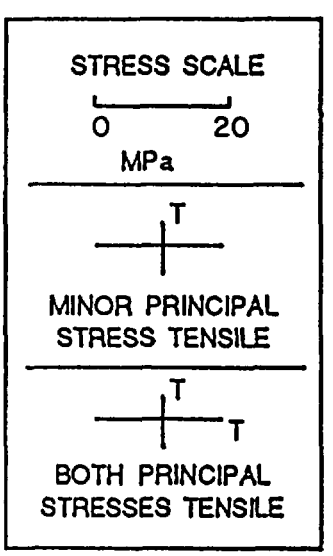

Figure 19. Principal Stresses Around the Access Ramp, with the Lower Initial Stress State (Case 1)

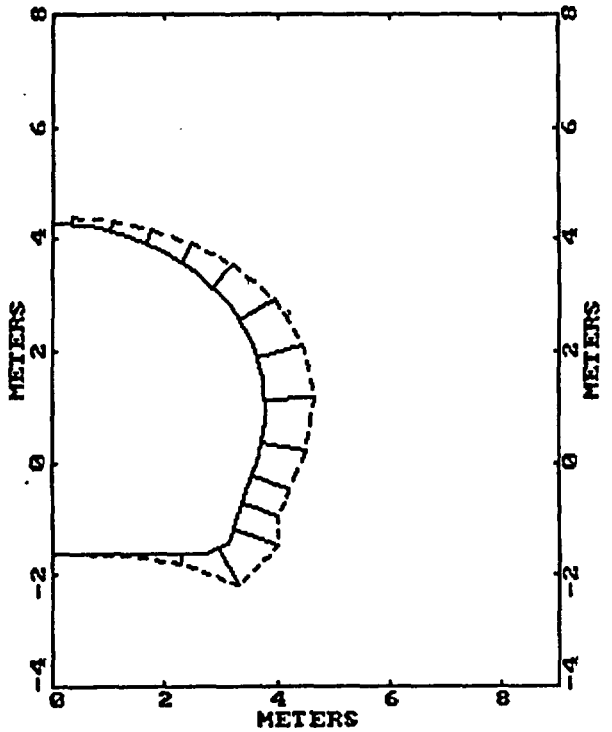

a) Case 1 after 10 yrs at x=-100 m

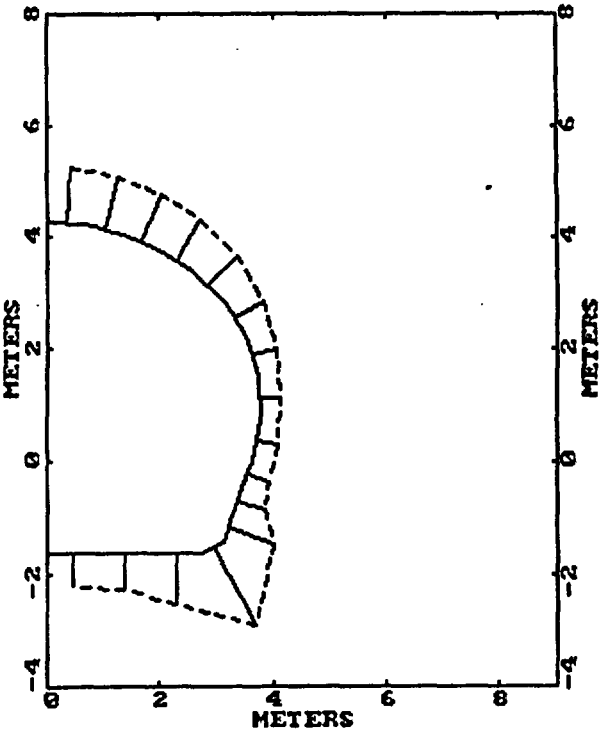

b) Case 1 after 50 yrs at x=-100 m

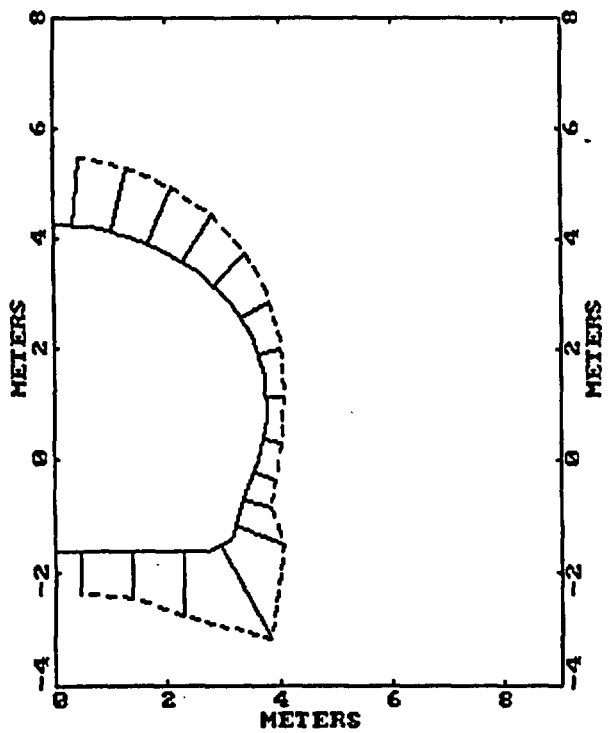

c) Case 1 after 100 yrs at x=-100 m

Tangential Stress

30 MPa

Note that a vector pointing out of the Opening Indicates a Compressive Stress.

Figure 20. Variation of Tangential Stress Around the Boundary of the Access Ramp where it Enters the Repository Horizon within the Shaft Pillar. The Lower Initial Stress State (Case 1) has been assumed.

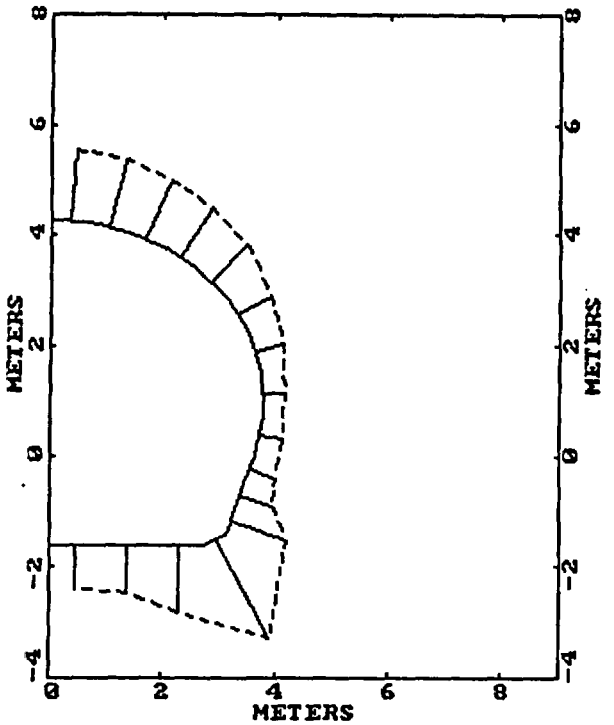

a) Case 2 after 10 yrs at x=-100 m

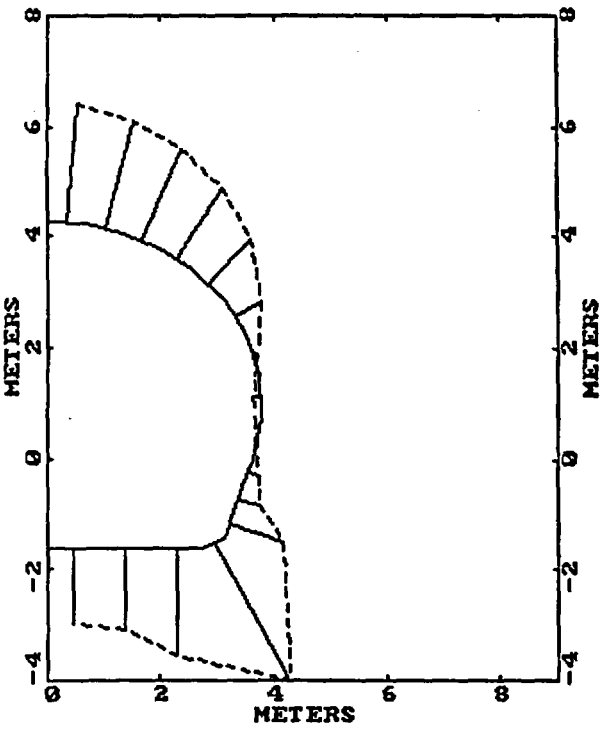

b) Case 2 after 50 yrs at x=-100 m

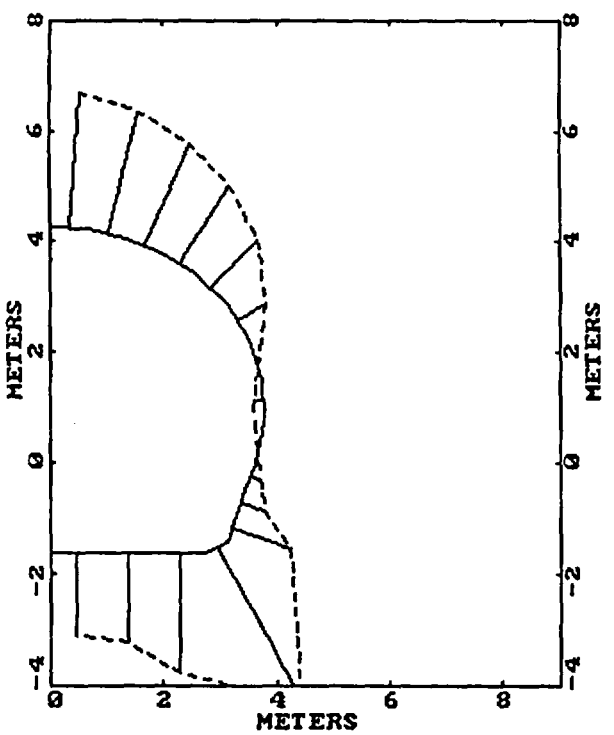

c) Case 2 after 10 yrs at x=-100 m

Tangential Stress

30 MPa

Note that a vector pointing out of the Opening Indicates a Compressive Stress.

Figure 21. Variation of Tangential Stress Around the Boundary of the Access Ramp Where it Reads the Repository Horizon within the Shaft Pillar. The Higher Initial Stress State (Case 2) has been assumed.

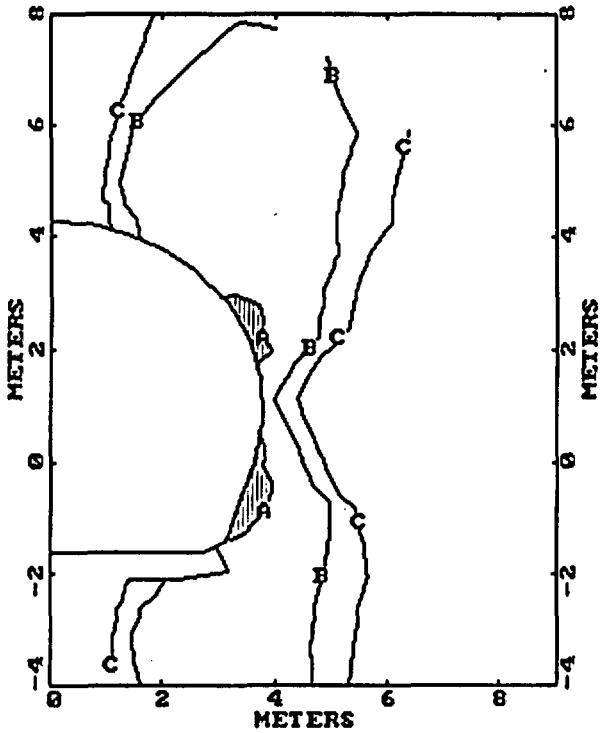

a) Case 1 after 10 yrs at x=-100 m

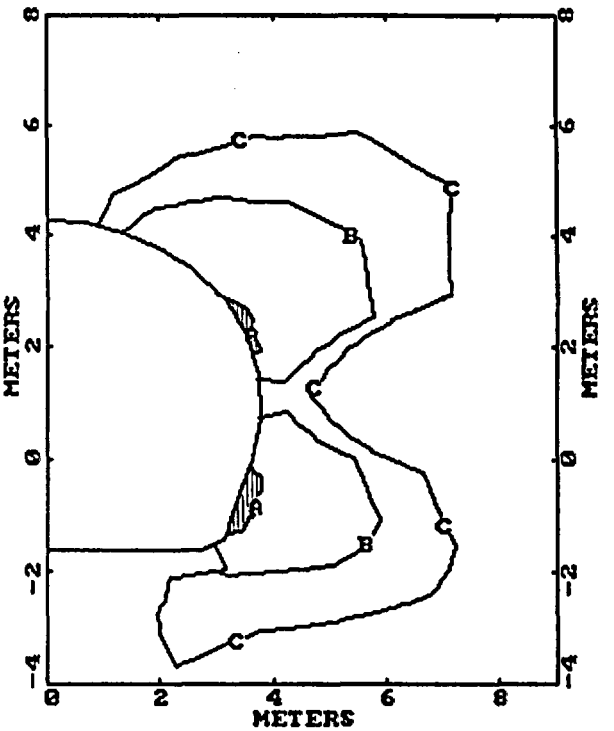

b) Case 1 after 50 yrs at x=-100 m

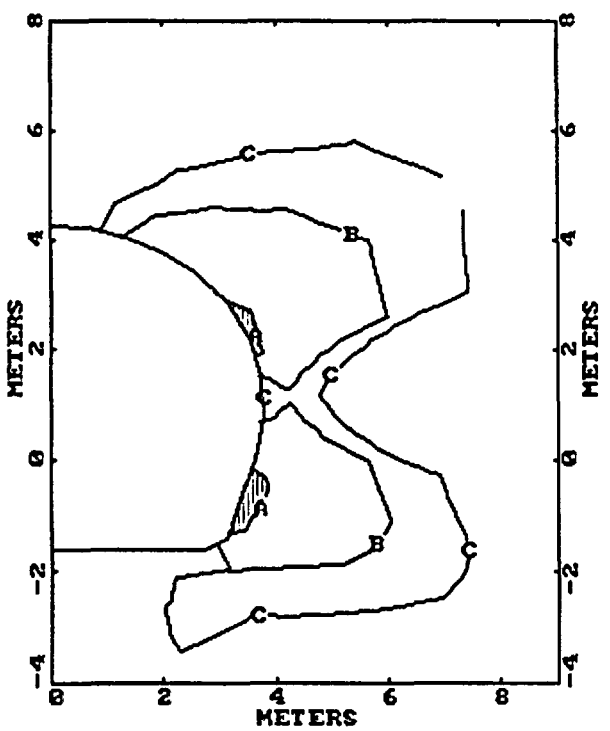

c) Case 1 after 100 yrs at x=-100 m

Ratio of Joint Shear Strength to Shear Stress

A - 1.0
B - 3.0
C - 5.0

Potential Joint Activation

Figure 22. Joint Activation Evaluation for the Access Ramp Where it Reaches the Repository Horizon, within the Shaft Pillar. The Lower Initial Stress State (Case 1) has been assumed.

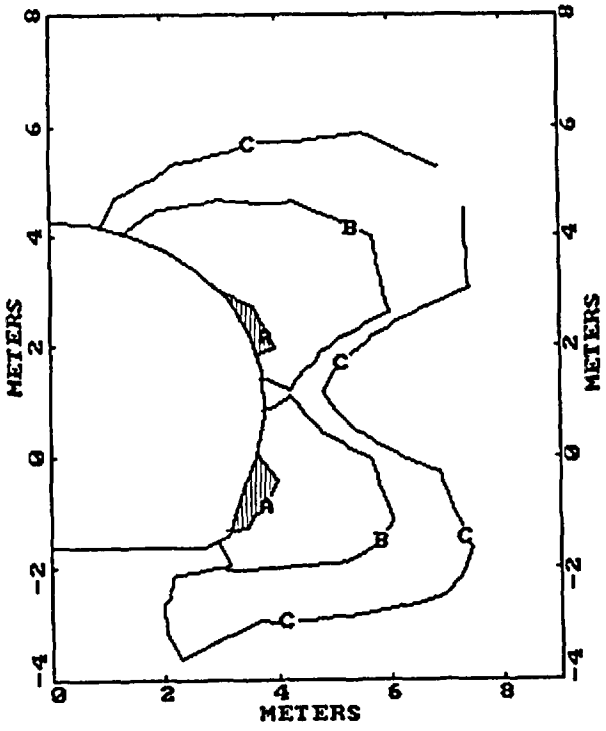

a) Case 2 after 10 yrs at x=-100 m

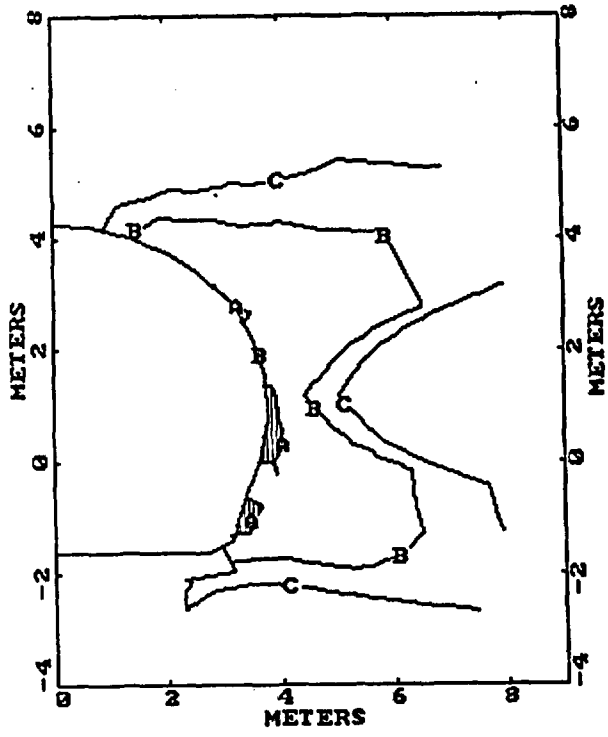

b) Case 2 after 50 yrs at x=-100 m

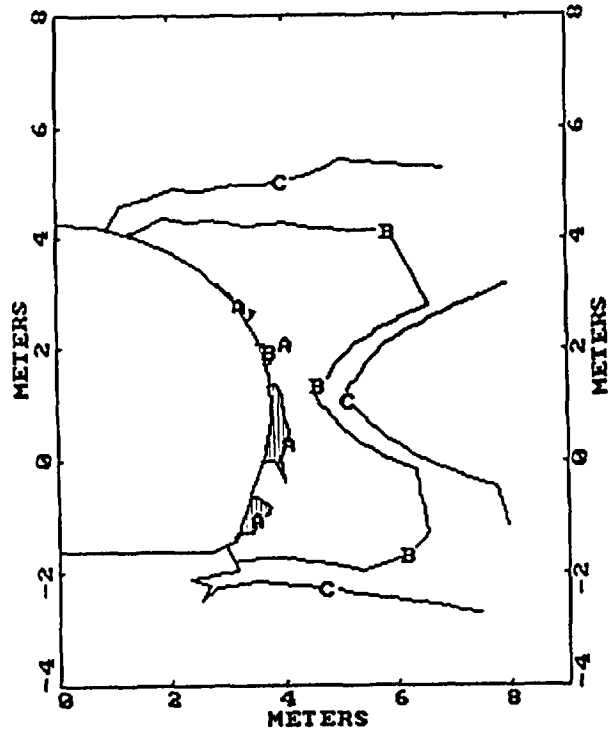

c) Case 2 after 100 yrs at x=-100 m

Ratio of Joint Shear
Strength to Shear Stress

A - 1.0
B - 3.0
C - 5.0

Potential Joint
Activation

Figure 23. Joint Activation Evaluation for the Access Ramp Where it Reaches the Repository Horizon, within the Shaft Pillar. The Higher Initial Stress State (Case 2) has been assumed.

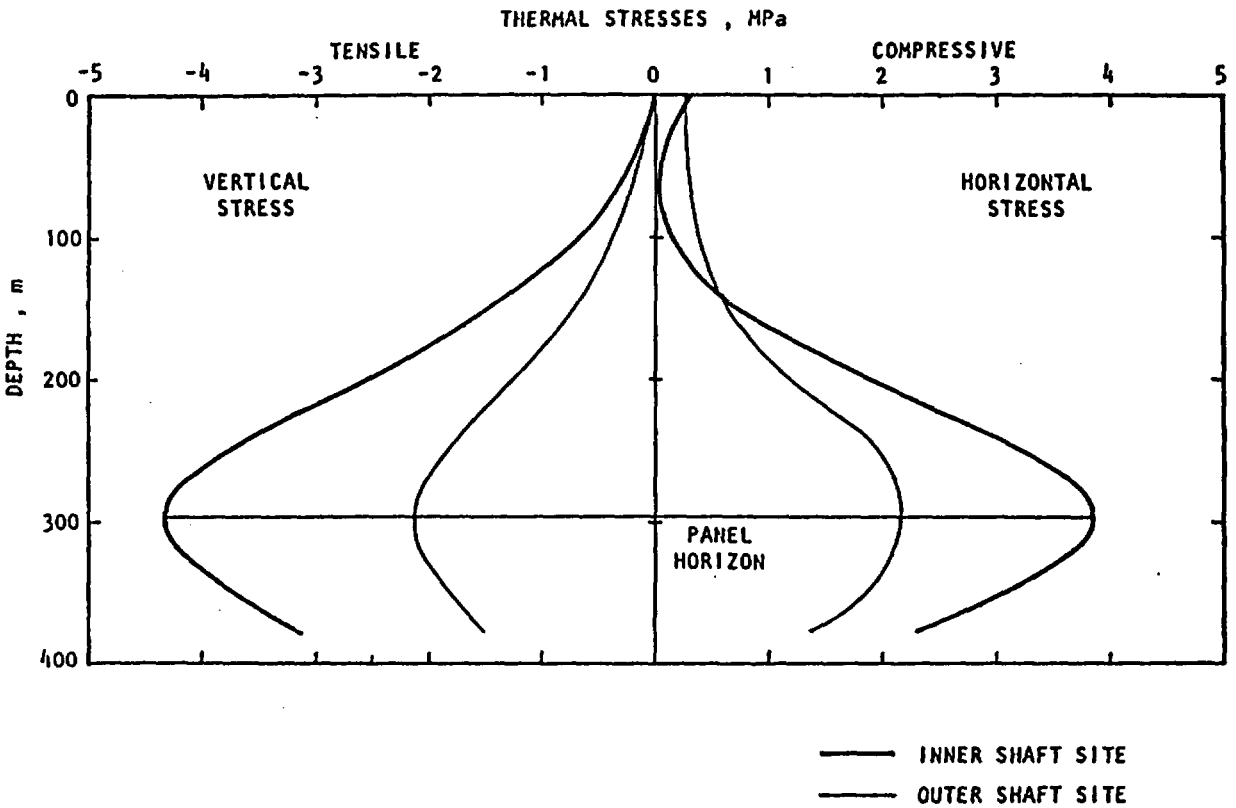

Figure 24. In-Plane Thermally Induced Stresses along Shaft at Site

Appendix A

Relationship of Data Used in this Analysis to NNWSI Reference Information Base

This preliminary design analysis was done to determine if significant differences exist in the response of shafts and ramps to excavation and thermal-induced stresses depending upon their location and the initial state of stress. As such, it is the comparison of the relative response of shafts and ramps to the changes in location and stress that is important rather than the absolute response of either. Any concerns over the representativeness of the data used in this report should effect the response of both shafts and ramps similarly and therefore should not change the conclusions of this report.

This analysis was initiated before baseline project data was established (Zeuch and Eatough, 1986); however, the data used was chosen because at the time it was the best estimate of what would become reference information. The data used are given in the table below, together with the reference data.

None of the data used by this report that is not already in the RIB is candidate information for inclusion in the RIB and none of the results of this work is candidate information for inclusion in the RIB. This report also does not present any new data to be input into the DRMS.

Table A-1:

Material Properties Data Used for This Analysis and RIB Data

TSw2 Property	Value	RIB Section	Data Used[1]		
Thermal Conductivity	2.07	1.3.1.6.4	1.85	(2)	W/m-deg. C
Heat Capacity	2.25	1.3.1.6.2	2.17	(2)	MJ/cu. m
Density	2.34	1.3.1.5.2	2.093	(2)	g/cu. cm
Poisson's Ratio	0.20	1.3.1.7.2	0.20		
Elastic Modulus	15.1	1.3.1.7.1	15.1		GPa
Coefficient Thermal Expansion	10.7	1.3.1.6.1	10.7		10^{-6}/deg. C
Rock Matrix Cohesion	22.1	1.3.1.7.6	22.1		MPa
Matrix Friction Angle	29.2	1.3.1.7.5	29.2		deg.
Tensile Strength	-9.0	1.3.1.7.4	-6.5	(3)	MPa
Joint Cohesion	1.0	1.3.1.8.1	1.0		MPa
Joint Friction Angle	38.7	1.3.1.8.1	38.7		deg.
Joint Orientation	---		V	(4)	

(1) Data, except as noted, from Nimick et al. (1984).
(2) Value chosen as representative of overburden material not just Tsw2. This was calculated using data from Nimick et al. (1984) by taking a weighted average of properties of units in overburden.
(3) Pre RIB value in initial draft of Nimick et al. (1984). Conclusions drawn in this analysis are not affected by this value because there are no regions where tension cracks would develop, even if this lower value pertained.
(4) Vertical joints (Johnstone, et al., 1984).

APPENDIX A REFERENCES

Johnstone, J. K., R. R. Peters, and P. F. Gnirk, "Unit Evaluation at Yucca Mountain, Nevada Test Site: Summary Report and Recommendation," SAND83-0372, Sandia National Laboratories, Albuquerque, NM, 1984.

Nimick, F. B., S. J. Bauer and J. R. Tillerson, "Recommended Matrix and Rock Mass Bulk, Mechanical Properties for Thermomechanical Stratigraphy of Yucca Mountain," Version 1, Keystone Document Number 6310-85-1, Division 6314, Sandia National Laboratories, Albuquerque, NM, 1984.

Zeuch, D. H. and M. J. Eatough, "Draft Reference Information Base for the Nevada Nuclear Waste Storage Investigations Project," Sandia National Laboratories, Albuquerque, NM, April, 1986.

APPENDIX B

RELATIONSHIP OF DATA USED IN THIS ANALYSIS TO SEPDB AND RIB

No data contained in this report is candidate information for the Site and Engineering Properties Data Base and/or the Reference Information Base.

APPENDIX C

DISTRIBUTION LIST

DISTRIBUTION LIST

D. H. Alexander (RW-232)
Office of Civilian Radioactive
Waste Management
U.S. Department of Energy
Forrestal Building
Washington, DC 20585

Eric Anderson
Mountain West Research-Southwest, Inc.
398 South Mill Avenue, Suite 300
Tempe, AZ 85281

J. H. Anttonen
Deputy Assistant Manager for
Commercial Nuclear Waste
Basalt Waste Isolation Project Office
U.S. Department of Energy
P.O. Box 550
Richland, WA 99352

Timothy G. Barbour
Science Applications
International Corporation
1626 Cole Boulevard, Suite 270
Golden, CO 80401

E. P. Binnall
Field Systems Group Leader
Building 50B/4235
Lawrence Berkeley Laboratory
Berkeley, CA 94720

R. J. Blaney (RW-22)
Office of Geologic Repositories
U.S. Department of Energy
Forrestal Building
Washington, DC 20585

P.M. Bodin (12)
Office of Public Affairs
U.S. Department of Energy
P.O. Box 98518
Las Vegas, NV 89193-8518

E. S. Burton (RW-25)
Siting Division
Office of Geologic Repositories
U.S. Department of Energy
Forrestal Building
Washington, DC 20585

Flo Butler
Los Alamos Technical Associates
1650 Trinity Drive
Los Alamos, New Mexico 87544

V. J. Cassella (RW-222)
Office of Civilian Radioactive
Waste Management
U.S. Department of Energy
Forrestal Building
Washington, DC 20585

B. W. Church
Director
Health Physics Division
U.S. Department of Energy
P.O. Box 14100
Las Vegas, NV 89114

C. R. Cooley (RW-24)
Geosciences & Technology Division
Office of Geologic Repositories
U.S. Department of Energy
Forrestal Building
Washington, DC 20585

J. A. Cross
Manager
Las Vegas Branch
Fenix & Scisson, Inc.
P.O. Box 14308
Mail Stop 514
Las Vegas, NV 87114

H. D. Cunningham
General Manager
Reynolds Electrical &
Engineering Co., Inc.
P.O. Box 14400
Mail Stop 555
Las Vegas, NV 89114

Neal Duncan (RW-44)
Office of Policy, Integration, and
Outreach
U.S. Department of Energy
Forrestal Building
Washington, DC 20585

J. J. Fiore (RW-221)
Office of Civilian Radioactive
Waste Management
U.S. Department of Energy
Forrestal Building
Washington, DC 20585

John Fordham
Desert Research Institute
Water Resource Center
P.O. Box 60220
Reno, NV 89506

Judy Foremaster (5)
City of Caliente
P.O. Box 158
Caliente, NV 89008

D. L. Fraser
General Manager
Reynolds Electrical & Engineering
Co., Inc.
P.O. Box 14400
Mail Stop 555
Las Vegas, NV 89114-4400

M. W. Frei (RW-231)
Office of Civilian Radioactive
Waste Management
U.S. Department of Energy
Forrestal Building
Washington, DC 20585

B. G. Gale (RW-223)
Office of Civilian Radioactive
Waste Management
U.S. Department of Energy
Forrestal Building
Washington, DC 20585

R. W. Gale (RW-40)
Office of Civilian Radioactive
Waste Management
U.S. Department of Energy
Forrestal Building
Washington, DC 20585

V. M. Glanzman
U.S. Geological Survey
913 Federal Center
P.O. Box 25046
Denver, CO 80225

Vincent Gong
Technical Project Officer for NNWSI
Reynolds Electrical & Engineering
Co., Inc.
P.O. Box 14400
Mail Stop 615
Las Vegas, NV 89114-4400

A. E. Gurrola
General Manager
Energy Support Division
Holmes & Narver, Inc.
P.O. Box 14340
Mail Stop 580
Las Vegas, NV 89114

R. Harig
Parsons Brinckerhoff Quade &
Douglas, Inc.
1625 Van Ness Avenue
San Franciso, CA 94109-3678

Roger Hart
Itasca Consulting Group, Inc.
P.O. Box 14806
Minneapolis, Minnesota 55414

T. Hay
Executive Assistance
Office of the Governor
State of Nevada
Capitol Complex
Carson City, NV 89710

L. R. Hayes (3)
Technical Project Officer for NNWSI
U.S. Geological Survey
421 Federal Center
P.O. Box 25046
Denver, CO 80225

W.M. Hewitt
Program Manager
Roy F. Weston, Inc.
955 L'Enfant Plaza, Southwest
Suite 800
Washington, DC 20024

T. H. Isaacs (RW-22)
Office of Civilian Radioactive
Waste Management
U.S. Department of Energy
Forrestal Building
Washington, DC 20585

Allen Jelacic (RW-233)
Office of Civilian Radioactive
Waste Management
U.S. Department of Energy
Forrestal Building
Washington, DC 20585

C. H. Johnson
Technical Program Manager
Nuclear Waste Project Office
State of Nevada
Evergreen Center, Suite 252
1802 North Carson Street
Carson City, NV 89701

S. H. Kale (RW-20)
Office of Civilian Radioactive
Waste Management
U.S. Department of Energy
Forrestal Building
Washington, DC 20585

B. J. King (2)
Librarian
Basalt Waste Isolation Project
Library
Rockwell Hanford Operations
P.O. Box 800
Richland, WA 99352

Cy Klingsberg (RW-24)
Office of Geologic Repositories
Geosciences and Technology Division
U.S. Department of Energy
Forrestal Building
Washington, DC 20585

J. P. Knight (RW-24)
Office of Civilian Radioactive
Waste Management
U.S. Department of Energy
Forrestal Building
Washington DC 20585

T. P. Longo (RW-25)
Office of Geologic Repositories
U.S. Department of Energy
Forrestal Building
Washington, DC 20585

R.R. Loux, Jr. (3)
Executive Director
Nuclear Waste Project Office
State of Nevada
Evergreen Center, Suite 252
1802 North Carson Street
Carson City, NV 89701

S. A. Mann
Manager
Crystalline Rock Project Office
U.S. Department of Energy
9800 South Cass Avenue
Argonne, IL 60439

Dr. Martin Mifflin
Desert Research Institute
Water Resources Center
2505 Chandler Avenue
Suite 1
Las Vegas, NV 89120

D. F. Miller
Director
Office of Public Affairs
U.S. Department of Energy
P.O. Box 98518
Las Vegas, NV 89193-8518

R. Lindsay Mundell
U.S. Bureau of Mines
Denver Federal Center
P.O. Box 25086
Building 20
Denver, Colorado 80225

S. D. Murphy
Technical Project Officer for NNWSI
Fenix & Scisson, Inc.
P.O. Box 15408
Mail Stop 514
Las Vegas, NV 89114

J. O. Neff
Manager
Salt Repository Project Office
U.S. Department of Energy
505 King Avenue
Columbus, OH 43201

D. C. Newton (RW-23)
Engineering & Licensing Division
U.S. Department of Energy
Forrestal Building
Washington, DC 20585

N.A. Norman
Project Manager
Bechtel National Inc.
P.O. Box 3965
San Francisco, CA 94119

D. T. Oakley (4)
Technical Project Officer for NNWSI
Los Alamos National Laboratory
P.O. Box 1663
Mail Stop F-619
Los Alamos, NM 87545

O. L. Olson
Manager
Basalt Waste Isolation Project Office
Richland Operations Office
U.S. Department of Energy
P.O. Box 550
Richland, WA 99352

Gerald Parker (RW-241)
Office of Civilian Radioactive
Waste Management
U.S. Department of Energy
Forrestal Building
Washington, DC 20585

David K. Parrish
RE/SPEC Inc.
3815 Eubank, N.E.
Albuquerque, NM 87191

J. P. Pedalino
Technical Project Officer for NNWSI
Holmes & Narver, Inc.
P.O. Box 14340
Mail Stop 605
Las Vegas, NV 89114

P. T. Prestholt
NRC Site Representative
1050 East Flamingo Road
Suite 319
Las Vegas, NV 89109

W. J. Purcell (RW-20)
Associate Director
Office of Civilian Radioactive
Waste Management
U.S. Department of Energy
Forrestal Building
Washington, DC 20585

L. D. Ramspott (3)
Technical Project Officer for NNWSI
Lawrence Livermore National
Laboratory
P.O. Box 808
Mail Stop L-204
Livermore, CA 94550

J. R. Rollo
Deputy Assistant Director
for Engineering Geology
U.S. Geological Survey
106 National Center
12201 Sunrise Valley Drive
Reston, VA 22092

B. C. Rusche (RW-1)
Director
Office of Civilian Radioactive
Waste Management
U.S. Department of Energy
Forrestal Building
Washington, DC 20585

J. E. Shaheen (RW-44)
Outreach Programs
Office of Policy, Integration and
Outreach
U.S. Department of Energy
Forrestal Building
Washington, DC 20585

Dr. Madan M. Singh
President
Engineers International, Inc.
98 East Naperville Road
Westmont, IL 60559-1595

M. E. Spaeth
Technical Project Officer for NNWSI
Science Applications
International Corporation
101 Convention Center Drive
Suite 407
Las Vegas, NV 89109

Christopher M. St. John
J.F.T. Agapito & Associates, Inc.
27520 Hawthorne Blvd., Suite 295
Rolling Hills Estates, CA 90274

Ralph Stein (RW-23)
Office of Civilian Radioactive
Waste Management
U. S. Department of Energy
Forrestal Building
Washington, DC 20585

K. Street, Jr.
Lawrence Livermore National
Laboratory
P.O. Box 808
Mail Stop L-209
Livermore, CA 94550

W. S. Twenhofel
Consultant
Science Applications
International Corp.
820 Estes Street
Lakewood, CO 89215

D. L. Vieth (4)
Director
Waste Management Project Office
U.S. Department of Energy
P.O. Box 98518
Las Vegas, NV 89193-8518

J. S. Wright
Technical Project Officer for NNWSI
Waste Technology Services Division
Westinghouse Electric Corporation
Nevada Operations
P.O. Box 708
Mail Strop 703
Mercury, NV 89023

Chief
Repository Projects Branch
Division of Waste Management
U.S. Nuclear Regulatory Commission
Washington, DC 20555

Document Control Center
Division of Waste Management
U.S. Nuclear Regulatory Commission
Washington, DC 20555

NTS Section Leader
Repository Project Branch
Division of Waste Management
U.S. Nuclear Regulatory Commission
Washington, DC 20555

SAIC-T&MSS Library (2)
Science Applications
International Corporation
101 Convention Center Drive
Suite 407
Las Vegas, NV 89109

ONWI Library
Battelle Columbus Laboratory
Office of Nuclear Waste Isolation
505 King Avenue
Columbus, OH 43201

Department of Comprehensive
Planning
Clark County
225 Bridger Avenue, 7th Floor
Las Vegas, NV 89155

Lincoln County Commission
Lincoln County
P.O. Box 90
Pioche, NV 89043

Community Planning and
Development
City of North Las Vegas
P.O. Box 4086
North Las Vegas, NV 89030

City Manager
City of Henderson
Henderson, NV 89015

Planning Department
Nye County
P.O. Box 153
Tonopah, NV 89049

Economic Development
Department
City of Las Vegas
400 East Stewart Avenue
Las Vegas, NV 89101

Director of Community Planning
City of Boulder City
P.O. Box 367
Boulder City, NV 89005

Technical Information Center
Roy F. Weston, Inc.
955 L'Enfant Plaza, Southwest
Suite 800
Washington, DC 20024

Commission of the
European Communities
200 Rue de la Loi
B-1049 Brussels
BELGIUM

6300	R. W. Lynch
6310	T. O. Hunter
6310	NNWSI CF
6310	75/12462/0/Q3
6311	A. L. Stevens
6311	C. Mora
6311	V. Hinkel (2)
6312	F. W. Bingham
6313	T. E. Blejwas
6314	J. R. Tillerson
6314	S. J. Bauer
6314	L. S. Costin
6314	B. L. Ehgartner (10)
6314	R. J. Flores
6314	A. J. Mansure
6314	R. M. Robb
6314	R. E. Stinebaugh
6315	S. Sinnock
6316	R. B. Pope
6332	WMT Library (20)
6430	N. R. Ortiz
3141	S. A. Landenberger (5)
3151	W. L. Garner (3)
8024	P. W. Dean
3154-3	C. H. Dalin (28) for DOE/OSTI